

## Heavy seeds and the first black holes: Insights from the BRAHMA simulations

AKLANT K. BHOWMICK,<sup>1, 2, 3</sup> LAURA BLECHA,<sup>4</sup> PAUL TORREY,<sup>1, 2, 3</sup> LUKE ZOLTAN KELLEY,<sup>5</sup> PRIYAMVADA NATARAJAN,<sup>6, 7, 8</sup> RACHEL S. SOMERVILLE,<sup>9</sup> RAINER WEINBERGER,<sup>10</sup> ALEX M. GARCIA,<sup>1, 2, 3</sup> LARS HERNQUIST,<sup>11</sup> TIZIANA DI MATTEO,<sup>12</sup> JONATHAN KHO,<sup>1</sup> AND MARK VOGELSBERGER<sup>13</sup>

<sup>1</sup>Department of Astronomy, University of Virginia, 530 McCormick Road, Charlottesville, VA 22904

<sup>2</sup>Virginia Institute for Theoretical Astronomy, University of Virginia, Charlottesville, VA 22904, USA

<sup>3</sup>The NSF-Simons AI Institute for Cosmic Origins, USA

<sup>4</sup>Department of Astronomy, University of California Berkeley, Gainesville, FL 32611, USA

<sup>5</sup>Department of Astronomy, University of California Berkeley, CA 22904, USA

<sup>6</sup>Dept. of Astronomy, Yale University, 219 Prospect Street, New Haven, CT 06511, USA

<sup>7</sup>Dept. of Physics, 217 Prospect Street, Yale University, New Haven, CT 06511, USA

<sup>8</sup>Black Hole Initiative, Harvard University, 20 Garden Street, Cambridge, MA 02138, USA

<sup>9</sup>Center for Computational Astrophysics, Flatiron Institute, New York, NY 10010, USA

<sup>10</sup>Leibniz Institute for Astrophysics Potsdam (AIP), An der Sternwarte 16, 14482 Potsdam, Germany

<sup>11</sup>Harvard-Smithsonian Center for Astrophysics, Harvard University, Cambridge, MA 02138, USA

<sup>12</sup>McWilliams Center for Cosmology, Carnegie Mellon University, Pittsburgh, PA 15213, USA

<sup>13</sup>Department of Physics and Kavli Institute for Astrophysics and Space Research, Massachusetts Institute of Technology, Cambridge, MA 02139, USA

Submitted to ApJ

## ABSTRACT

From the luminous quasars at  $z \sim 6$  to the recent  $z \sim 9$ –11 AGNs revealed by JWST, observations of the earliest black hole (BH) populations can provide unique constraints on BH formation and growth models. We use the BRAHMA simulations with constrained initial conditions to investigate BH assembly in extreme overdense regions. The simulations implement heavy  $\sim 10^4$ – $10^5 M_\odot$  seeds forming in dense, metal-poor gas exposed to sufficient Lyman–Werner flux. With gas accretion modeled via Bondi–Hoyle formalism and BH dynamics and mergers with a subgrid dynamical friction scheme, we isolate the impact of seeding, dynamics, accretion, and feedback on early BH growth. With fiducial stellar and AGN feedback inherited from **IllustrisTNG**, accretion is strongly suppressed at  $z \gtrsim 9$ , leaving mergers as the dominant growth channel. Gas accretion dominates at  $z \lesssim 9$ , where permissive models (super-Eddington or low radiative efficiency) build  $\sim 10^9 M_\odot$  BHs powering quasars by  $z \sim 6$ , while stricter **IllustrisTNG**-based prescriptions yield much lower BH masses ( $\sim 10^6$ – $10^8 M_\odot$ ). Our seed models strongly affect merger-driven growth at  $z \gtrsim 9$ : only the most lenient models (with  $\sim 10^5 M_\odot$  seeds) produce enough BH mergers to reach  $\gtrsim 10^6 M_\odot$  by  $z \sim 10$ , consistent with current estimates for GN-z11. Our dynamical friction model gives low merger efficiencies, hindering the buildup of  $\gtrsim 10^7 M_\odot$  BHs by  $z \sim 9$ –10, as currently inferred for GHZ9, UHZ1, and CAPERS-LRD-z9. If the BH-to-stellar mass ratios of these sources are indeed as extreme as currently inferred, they would require either very short BH merger timescales or reduced AGN thermal feedback. Weaker stellar feedback boosts both star formation and BH accretion and cannot raise these ratios.

**Keywords:** Galaxy formation (595), Hydrodynamical simulations (767), Supermassive black holes (1663), Active galactic nuclei (16)

## 1. INTRODUCTION

Corresponding author: Aklant K. Bhowmick  
 aklant.app@gmail.com

Over the past three decades, numerous observational efforts with the Sloan Digital Sky Survey, Pan-STARRS1, Wide-field Infrared Survey Explorer (WISE)

and several others have discovered a population of the brightest quasars (bolometric luminosities  $L_{\text{bol}} \sim 10^{47} \text{ erg s}^{-1}$ ) at high redshifts ( $z \sim 4 - 7$ ; Fan et al. 2001; Willott et al. 2010; Mortlock et al. 2011; Venemans et al. 2015; Jiang et al. 2016; Bañados et al. 2016; Reed et al. 2017; Matsuoka et al. 2018; Wang et al. 2018; Bañados et al. 2018; Matsuoka et al. 2019; Yang et al. 2019; Wang et al. 2021). More recently, the James Webb Space Telescope (JWST) has revealed a large population of low luminosity Active Galactic Nuclei (AGN) at  $z \sim 4 - 7$  (Onoue et al. 2023; Harikane et al. 2023; Kocevski et al. 2023; Maiolino et al. 2023; Larson et al. 2023; Greene et al. 2023; Kocevski et al. 2024; Andika et al. 2024; Akins et al. 2024). JWST is also pushing the redshift frontier for AGN by detecting a handful of objects at  $z \sim 9 - 11$ . These include spectroscopically confirmed objects such as CEERS-1019 (Larson et al. 2023), GN-z11 (Maiolino et al. 2024); UHZ1 (Bogdán et al. 2024; Goulding et al. 2023), GHZ9 (Kovács et al. 2024) and CAPERS-LRD-z9 (Taylor et al. 2025). Notably, UHZ1 and GHZ9 are also found to have X-ray counterparts in *Chandra*. These early AGN detected by JWST, together with the bright  $z \sim 6$  quasars, offer the possibility of stringent constraints on early BH formation and growth models.

Natural candidates for the first “seeds” of SMBHs include remnants of Population III (Pop III) stars (Fryer et al. 2001; Madau & Rees 2001; Xu et al. 2013; Smith et al. 2018). These “light Pop III seeds” are expected to be around  $\sim 100 M_{\odot}$ . But the discovery of the  $z \gtrsim 6$  quasars suggested the existence of more massive BH seeds, since forming the  $\sim 10^9 M_{\odot}$  BHs that power them would otherwise require prolonged and steady super-Eddington accretion from light seeds. The postulated massive seeding channels include “intermediate-mass seeds” in dense nuclear star clusters born out of runaway stellar and BH mergers (Davies et al. 2011; Lupi et al. 2014; Kroupa et al. 2020; Das et al. 2021b,a) or gas accretion (Alexander & Natarajan 2014; Natarajan 2021), and “heavy seeds” ( $\sim 10^4 - 10^5 M_{\odot}$ ) as direct collapse black holes or DCBHs (Bromm & Loeb 2003; Begelman et al. 2006; Regan et al. 2014; Latif et al. 2016; Luo et al. 2018; Wise et al. 2019; Luo et al. 2020; Begelman & Silk 2023). While the heaviest DCBH seeds have traditionally been believed to be rare due to the strong critical Lyman Werner (LW) fluxes that may be required for their formation ( $J_{\text{crit}} \gtrsim 1000 J_{21}$ , where  $J_{21} = 10^{-21} \text{ erg s}^{-1} \text{ cm}^{-2} \text{ Hz}^{-1}$ ; Regan et al. 2014; Agarwal et al. 2016) in dense pristine gas, their large initial masses make them compelling candidates for the origins of the  $z \gtrsim 6$  quasars.

The abundance of JWST AGN at  $z \sim 4 - 7$ , if they all originated from heavy seeds, however, suggests that heavy seed formation may not be as rare or inefficient as previously believed. This is because the canonical LW flux-based channel for DCBH formation predicts number densities of  $\sim 10^{-6} \text{ Mpc}^{-3}$  even for moderate values of the critical flux ( $J_{\text{crit}} \sim 300 J_{21}$ ; Habouzit et al. 2016, O’Brennan et al. 2025 – which is  $\sim 10 - 100$  times smaller than the measured luminosity functions of the JWST AGN; Kokorev et al. 2024, Greene et al. 2024, Akins et al. 2024). These suggested over-abundances of JWST AGNs may therefore be indicative of additional formation channels for heavy seeds in operation in the early Universe that may not require such stringent LW flux requirements. Relatedly, there are several theoretical works that have suggested that DCBH formation could be enhanced if there are additional processes to keep the gas from cooling and fragmenting, such as dynamical heating (Wise et al. 2019; Regan et al. 2020b,a) or magnetic fields (Latif et al. 2023).

Additionally, many of the JWST AGN have been estimated to have significantly higher BH mass to host stellar mass ratios compared to the local scaling relations (Kokorev et al. 2023; Bogdán et al. 2024; Natarajan et al. 2024; Kokorev et al. 2024; Kocevski et al. 2024; Durodola et al. 2024; Juodžbalis et al. 2025). Such “over-massive” BHs are predicted to be a key signature of heavy seeds (Natarajan et al. 2017; Visbal & Haiman 2018; Scoggins et al. 2023; Natarajan et al. 2024; Scoggins & Haiman 2024). But it is also important to keep in mind that the BH mass and host galaxy stellar mass measurements from current JWST observations carry significant uncertainties, as discussed further in Section 4.5.

The highest redshift ( $z \sim 9 - 11$ ) JWST AGN are also expected to be rare objects. It is therefore reasonable to expect that the  $z \sim 9 - 11$  AGNs and  $z \sim 6 - 7$  quasar populations originate from similarly rare (and highly overdense) peaks in the initial matter density field. In fact, several theoretical models aimed at assembling  $\gtrsim 10^9 M_{\odot}$  quasars by  $z \sim 6$  also produce  $\sim 10^6 - 10^8 M_{\odot}$  BHs by  $z \sim 9 - 11$ , comparable to the masses inferred for the JWST-detected AGN (Valiante et al. 2016; Sassano et al. 2021; Zhu et al. 2022; Bhowmick et al. 2022b; Bennett et al. 2024). This could also suggest that at least some of these JWST AGN are possibly progenitors of the  $z \sim 6$  quasars. However, we do note that in several simulations, notably, BlueTides & the ASTRID simulation suite have shown that the most massive BH at early times does not necessarily remain the most massive one at later epochs, as the cosmic environment strongly influences BH growth (Di Matteo et al. 2008). In partic-

ular, BH merger trees show that the rank order of BH masses reshuffles significantly over cosmic time. Tracking the evolution of BH populations, it has been found that the most massive BH at  $z \sim 8$  for instance often does not correspond to the most massive BH at either  $z = 4$  or  $z = 0$  (Ni et al. 2022; Bird et al. 2022).

Semi-analytic models (SAMs) have been widely used to study high- $z$  quasars, as their low computational cost offers a significant advantage over cosmological simulations to explore these rare BH populations in extreme overdense environments (Valiante et al. 2016; Sassano et al. 2021; Trinca et al. 2022, 2024; Jeon et al. 2025). However, without tracking the gas hydrodynamics, it is much more difficult to explicitly model the interaction between stellar feedback and BH accretion in SAMs.

Several cosmological simulations (Habouzit et al. 2017; Byrne et al. 2023), as well as very recent small-scale “resolved physics” simulations (Partmann et al. 2025; Petersson et al. 2025), have shown that in addition to self-regulation from AGN feedback, stellar feedback may also play a significant role in regulating BH accretion in low-mass galaxies at high  $z$ . As a result, there can be substantial differences in the mass assembly histories predicted by SAMs and simulations. For example, in the GAMETE-QSO SAM used by Valiante et al. (2016) and Sassano et al. (2021), the growth of BH becomes dominated by accretion as early as  $z \sim 15$ , whereas in our earlier simulations (Bhowmick et al. 2022b) using **Illustris-TNG** physics, this transition occurs significantly later (around  $z \sim 9 - 10$ ). Although the accretion history is critically influenced by the choice of accretion model, both GAMETE-QSO and **Illustris-TNG**, we note, adopt Bondi-Hoyle accretion. The delayed onset of accretion-dominated BH growth can significantly influence which combinations of seeding and accretion models are viable for producing early BHs. Furthermore, it could pose an even greater challenge in assembling the currently measured masses of  $z \sim 9 - 11$  JWST AGN.

In cosmological simulations, the assembly of the earliest black holes (BHs) is typically studied either by ‘zooming in’ on a specific target halo within large volumes (Sijacki et al. 2009; Costa et al. 2014; Zhu et al. 2022; Bennett et al. 2024), or by constraining the initial conditions within smaller boxes (Huang et al. 2020; Ni et al. 2022; Bhowmick et al. 2022b). These simulations have successfully assembled high- $z$  quasars, particularly using heavy ( $\gtrsim 10^4 M_\odot$ ) BH seeds. However, most of these studies adopt BH repositioning, that is, artificially pinning BHs to local potential minima, to stabilize their dynamics, since these simulations typically cannot resolve the dynamical friction (DF) force of the BH. This repositioning can artificially increase BH growth by en-

hancing both BH-BH mergers and gas accretion. In addition, many of the above simulations initially seed BHs using a simple halo-mass threshold. These seeding models do not correspond to any of the physically motivated BH formation channels. The use of simplified BH seeding and dynamics models makes it difficult to constrain the origins of these extreme high-redshift BHs, even if they are successfully reproduced in simulations. Moreover, most of these studies were carried out before the discovery of AGN at  $z \sim 9 - 11$  by JWST.

Over the years, several subgrid models have been introduced to account for unresolved BH dynamical friction (e.g., Tremmel et al. 2015; Pfister et al. 2019; Chen et al. 2022; Ma et al. 2023; Damiano et al. 2024; Genina et al. 2024), and many large-volume cosmological simulations have begun to adopt them (Habouzit et al. 2017; Tremmel et al. 2017; Ni et al. 2024). Currently, some of these simulations have also moved beyond the traditional halo mass-based seeding approach by adopting more sophisticated seeding models that depend on local gas properties (Tremmel et al. 2017; Habouzit et al. 2017). Our previous work introduced a new family of gas-based seed models that account for local gas density, metallicity, Lyman-Werner flux, gas spin, and environment (Bhowmick et al. 2021, 2022a,b, 2024a). These efforts culminated in the creation of the **BRAHMA** simulation suite (Bhowmick et al. 2021, 2022a, 2024b,c, 2025a).

However, there is a lack of studies that systematically explore variations of gas-based seed models coupled with the more sophisticated dynamical friction models in constrained or zoom-in simulations specifically aimed at explaining the formation of rare, extreme BHs at early times. Even in our earlier work (Bhowmick et al. 2022b, hereafter B22), which examined the formation of  $z \sim 6$  quasars using gas-based seed models, BH repositioning was still employed — inevitably overestimating the contribution of early BH mergers to total BH growth. More generally, if we want to use high- $z$  BH observations to constrain BH seeding models in the future, we need to understand the impact of BH dynamics as well as other aspects of our BH and galaxy evolution model that impact BH growth, which include BH accretion, stellar and AGN feedback.

In this work, we use constrained simulations to jointly explore the impact of BH seeding, dynamics, accretion, stellar and AGN feedback on BH mass assembly in extreme overdense regions of the large-scale structure where we may expect  $z \sim 6$  quasars and  $z \sim 9 - 11$  JWST AGNs to reside. These simulations extend the **BRAHMA** framework by coupling its gas-based seed models with a sub-grid DF model for BH dynamics. We refer to these runs as the **BRAHMA-CONSTRAINED** simulations. For the

first time, we used a dynamical friction model to assemble early, extreme BHs under systematic variations of physically motivated gas-based seeding prescriptions.

The remainder of this manuscript is organized as follows. In Section 2, we describe the simulation setup and the BH modeling used. In Section 3, we present results for BH mass assembly under different models of BH seeding, dynamics, accretion, and stellar and AGN feedback, and discuss their implications for the current measurements of  $z \sim 6$  quasars and the JWST AGNs at  $z \sim 9-11$ . Section 4 connects our results to the broader literature and outlines caveats and future directions. Finally, Section 5 summarizes our main findings.

## 2. METHODS

Our new BRAHMA-CONSTRAINED simulations specifically target the rarest over-density peaks where we expect the  $z \gtrsim 6$  quasars to reside. These simulations used constrained initial conditions (ICs) designed to form massive  $\gtrsim 10^{12} M_{\odot}$  halos by  $z = 6$ . The simulations are run using the AREPO gravity + magnetohydrodynamics (MHD) code (Springel 2010; Pakmor et al. 2011, 2016; Weinberger et al. 2020). The code uses a PM Tree (Barnes & Hut 1986) solver for N-body gravity, coupled with an MHD solver that uses a dynamic unstructured grid generated via a Voronoi tessellation of the domain. The underlying cosmology is adopted from the Planck Collaboration et al. (2016) results, i.e.  $\Omega_{\Lambda} = 0.6911$ ,  $\Omega_m = 0.3089$ ,  $\Omega_b = 0.0486$ ,  $H_0 = 67.74 \text{ km s}^{-1}\text{Mpc}^{-1}$ ,  $\sigma_8 = 0.8159$ ,  $n_s = 0.9667$ . Our simulations are  $[13.3 \text{ Mpc}]^3$  in volume and most of our boxes use  $N_{\text{DM}} = 360^3$  DM particles with an equal number of initial gas cells simulated until  $z = 6$ . This default setup (hereafter referred to as “default resolution” boxes) achieves a mass resolution of  $M_{\text{DM}} = 1.5 \times 10^6 M_{\odot}$  for DM, a target gas mass resolution of  $2.3 \times 10^5 M_{\odot}$ , and a gravitational softening length of 0.73 kpc. Our gas mass resolution was targeted to resolve  $\sim 10^5 M_{\odot}$  BH seeds. This of course implies that the DM particles are 8 times larger than the seeds, which can disrupt their dynamics due to large gravitational kicks. As described later in section 2.4, we stabilize the BH dynamics by assigning a larger initial *dynamical mass* (for purposes of gravity calculation) to the BH seeds that is 2.4 times higher than the mass of DM particles. Additionally, we run boxes with 8 times higher number of particles ( $N_{\text{DM}} = 720^3$ ) to 1) test the impact of decreasing the seed mass to  $\sim 10^4 M_{\odot}$ , and to 2) isolate the dependence on resolution at the default seed mass of  $\sim 10^5 M_{\odot}$  (see Appendix A). These higher resolution boxes have a mass resolution of  $1.9 \times 10^5 M_{\odot}$  for DM and a target gas mass resolution of  $3 \times 10^4 M_{\odot}$ . However, the higher-resolution simula-

tions are run only down to  $z \sim 7-8$  as they are much more computationally expensive. As we show in Appendix A, the changes in resolution do not significantly impact our main conclusions.

In addition to the BH models, the BRAHMA-CONSTRAINED simulations incorporate most aspects of their underlying galaxy formation framework from the `IllustrisTNG` simulations (Pillepich et al. 2018a; Weinberger et al. 2017), which itself is a successor of the Illustris model (Vogelsberger et al. 2013; Torrey et al. 2014). The simulations account for gas cooling due to primordial species ( $\text{H}, \text{H}^+, \text{He}, \text{He}^+, \text{He}^{++}$ ), following the rates provided by Katz et al. 1996, while metal cooling is implemented using pre-computed tables based on gas density, temperature, metallicity, and redshift (Smith et al. 2008; Wiersma et al. 2009). Star formation occurs in gas cells that exceed a density threshold of  $0.13 \text{ cm}^{-3}$ . These cells generate star particles that represent single stellar populations (SSPs), characterized by their age, metallicity, and an initial mass function based on Chabrier (2003). The star-forming gas cells correspond to an unresolved multiphase interstellar medium (ISM), which is described using an effective equation of state (Springel & Hernquist 2003; Vogelsberger et al. 2014a). SSPs undergo stellar evolution as described in Vogelsberger et al. (2013), with specific modifications for `IllustrisTNG` outlined in Pillepich et al. (2018a). The simulations track chemical enrichment by following the evolution of seven metal species—C, N, O, Ne, Mg, Si, and Fe—alongside H and He. Stellar feedback, including that from Type Ia and Type II supernovae, is modeled as large-scale galactic winds (Pillepich et al. 2018b), which transport metals from SSPs into the surrounding gas.

### 2.1. Constrained Initial conditions

To produce rare overdense peaks in our small simulation volumes, we generated initial conditions using *constrained Gaussian realizations* (CR). The theoretical formalism was originally introduced by the Hoffman & Ribak (1991) and van de Weygaert & Bertschinger (1996), and we use its most recent implementation within the `GaussianCR` code developed by Huang et al. (2020) and Ni et al. (2022). The unique feature of the CR method is its ability to efficiently sample a Gaussian random field of over-density peaks, in a way that is conditioned on various (user-specified) large-scale features. The implementation of Ni et al. (2022) allows us to specify not just the peak height ( $\nu$ ) for the overdensity field (smoothed over a scale  $R_g$ ), but also its “higher order” features, including compactness and tidal field strength.

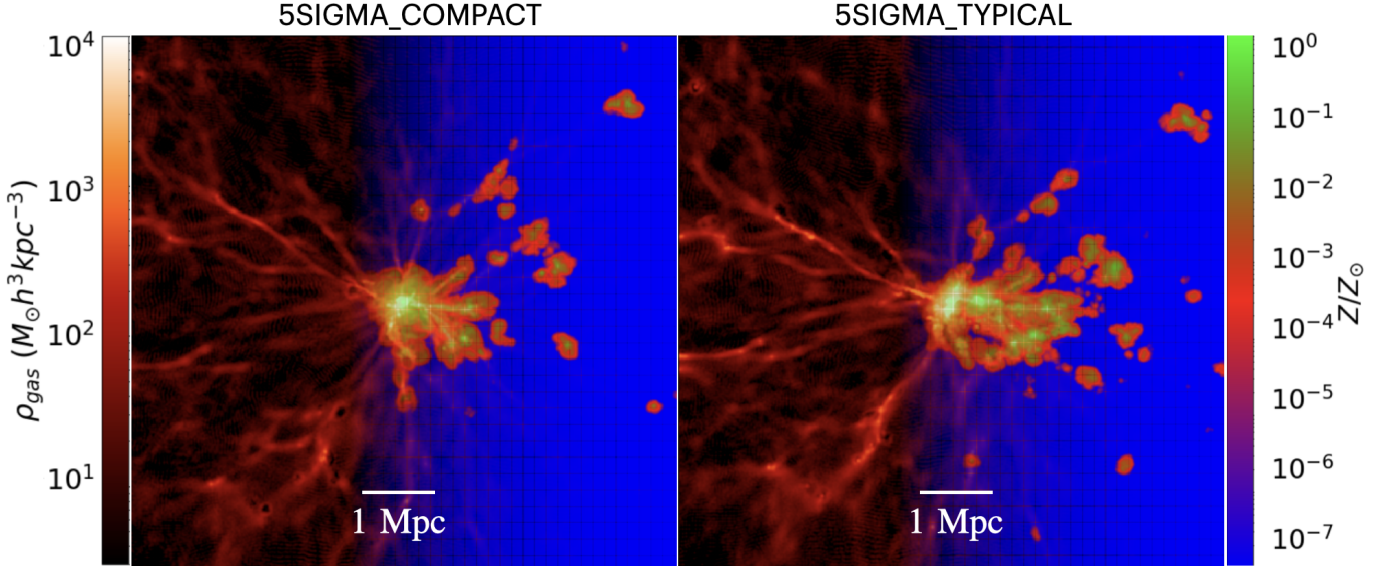


**Figure 1.** Visualization of our two different types of constrained simulation boxes at  $z = 6$ , showing the 2D gas density profile which gradually transitions into the 2D gas metallicity profile from left to right. At the center of each box, there is a  $5\sigma$  overdensity peak (when smoothed over 1 Mpc scales). In the left panel (5SIGMA\_COMPACT), the overdensity peak has significantly higher compactness and low tidal field strength compared to a typical  $5\sigma$  peak (5SIGMA\_TYPICAL) that is shown in the right panel. Both simulations produce a  $3 \times 10^{12} M_\odot$  halo at  $z = 6$ . Unless explicitly stated, most of the figures hereafter show results for 5SIGMA\_COMPACT simulations.

We will use two types of ICs with a  $5\sigma$  peak at scale  $R_g = 1 \text{ Mpc}/h$ . The vast majority of our boxes use the first type, referred to as 5SIGMA\_COMPACT, which has higher compactness and lower tidal field strength compared to typical values for a  $5\sigma$  peak. The use of 5SIGMA\_COMPACT is motivated by Ni et al. (2022), who found that, in addition to peak height, BH growth was strongest in peaks with high compactness and low tidal field strength. The 5SIGMA\_COMPACT IC is similar to one of the setups used by Ni et al. (2022), but our simulations adopt  $\sim 10$  times higher mass resolution over a volume  $\sim 11$  times smaller. While a smaller volume can in principle be a liability for adequately capturing the collapse of such an overdense region, we demonstrate in Appendix A that our results are not significantly impacted even when we adopt a volume  $\sim 8$  times larger. We also run one box with a more typical  $5\sigma$  peak, which adopts the most probable values of compactness and tidal field strength. In Figure 1, we show the density and metallicity fields at  $z = 6$  for both types of ICs. Each produces an extreme overdense peak at the box center where the constraint is imposed, leading to most of the star formation and metal enrichment occurring in its vicinity. Visually, the overdensity produced by 5SIGMA\_COMPACT is more compact and spherically symmetric than that of 5SIGMA\_TYPICAL.

Both ICs, by construction, form a  $\sim 3 \times 10^{12} M_\odot$  halo by  $z = 6$ , consistent with the observational es-

timate of Eilers et al. (2024) for high- $z$  quasar hosts based on quasar–galaxy cross-correlation measurements (see Figure 2, upper panel). Their stellar masses (bottom panel) at  $z = 6$  are of order  $\sim 10^{11} M_\odot$ , broadly consistent with JWST measurements for those quasars whose host galaxies have been identified (Ding et al. 2025). Notably, the halo formation time is earlier in 5SIGMA\_COMPACT. As a result, the progenitor halos at  $z \sim 9\text{--}11$  are significantly more massive in 5SIGMA\_COMPACT (a few  $\times 10^{11} M_\odot$ ) compared to 5SIGMA\_TYPICAL (a few  $\times 10^{10} M_\odot$ ). Incidentally, the  $z \sim 9\text{--}11$  stellar masses produced by 5SIGMA\_COMPACT are consistent with current measurements of CEERS-1019 and GN-z11, while those from 5SIGMA\_TYPICAL are consistent with estimates for UHZ1 and GHZ9. Therefore, our chosen ICs provide appropriate environments not only for the  $z \sim 6$  quasars, but also for the  $z \sim 9\text{--}11$  JWST AGNs. Most of our simulations use the 5SIGMA\_COMPACT IC, with a handful also using the 5SIGMA\_TYPICAL IC.

Note, however, that there is no strong evidence that the  $z \sim 6$  quasars and  $z \sim 9\text{--}11$  AGN inhabit the same environments, and current observational constraints for the host stellar masses remain uncertain. While our constrained simulations may implicitly suggest that both these populations reside in similar environments, these ICs are not intended to capture the full diversity of environments in which such objects may arise. Probing

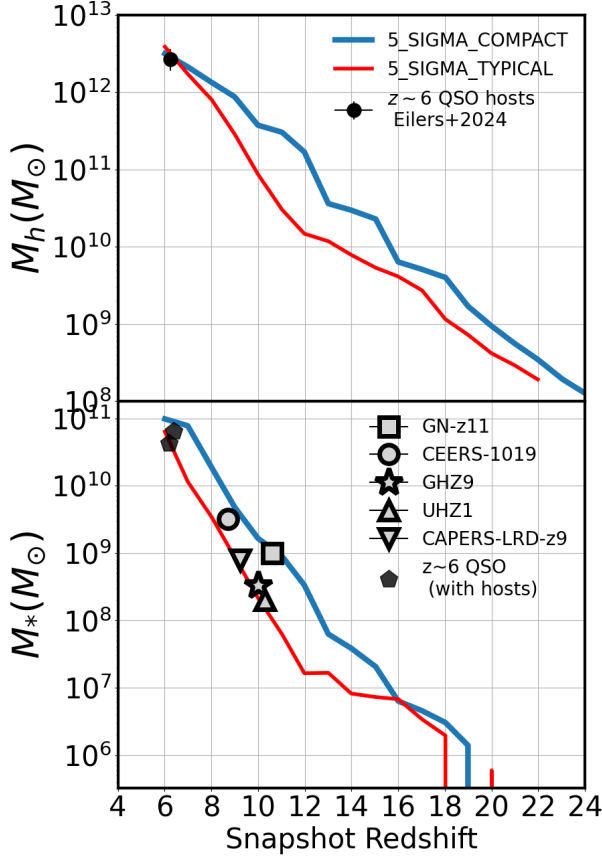


**Figure 2.** Evolution of the total mass (upper panel) and the stellar mass (lower panel) of the most massive halo across different redshift snapshots. The halo reaches a mass of  $\sim 3 \times 10^{12} M_{\odot}$  at  $z = 6$ , consistent with the observed  $z \sim 6$  quasars based on quasar-galaxy cross correlation measurements of Eilers et al. (2024) shown as black circles. The stellar masses are consistent with the current estimates of the JWST AGN hosts, which makes this region a promising site for studying the assembly of  $z \sim 9 - 11$  BHs.

this diversity will require applying our models to much larger-volume cosmological simulations (Zhou et al., in prep.). In contrast, our aim here is to simply examine BH assembly within a rare environment under varying model assumptions.

## 2.2. Black hole accretion and feedback

To model the accretion of gas onto BHs, we use the modified version of the Bondi-Hoyle formalism given by the equation:

$$\dot{M}_{\text{bh}} = \min(\dot{M}_{\text{Bondi}}, f_{\text{Edd}} \dot{M}_{\text{Edd}}) \quad (1)$$

$$\dot{M}_{\text{Bondi}} = \alpha \frac{4\pi G^2 M_{\text{bh}}^2 \rho}{c_s^3} \quad (2)$$

$$\dot{M}_{\text{Edd}} = \frac{4\pi G M_{\text{bh}} m_p}{\epsilon_r \sigma_T c} \quad (3)$$

where  $G$  is the gravitational constant,  $\rho$  is the local gas density,  $M_{\text{bh}}$  is the BH mass,  $c_s$  is the local sound speed,  $m_p$  is the proton mass, and  $\sigma_T$  is the Thompson scattering cross section. The accretion model has three free parameters that we have varied among our boxes: radiative efficiency  $\epsilon_r$ , the boost factor  $\alpha$ , and the Eddington factor  $f_{\text{Edd}}$  that determines the maximum accretion rate in units of the Eddington rate. The adopted radiative efficiency determines the bolometric luminosities given by  $L_{\text{bol}} = \epsilon_r \dot{M}_{\text{bh}} c^2$ , a fraction of which is coupled to the surrounding gas as AGN feedback. The AGN feedback has two modes that operate at different Eddington ratios  $\eta$ . At high Eddington ratios ( $\eta > \eta_{\text{crit}} \equiv \min[0.002(M_{\text{BH}}/10^8 M_{\odot})^2, 0.1]$ ), a fraction (thermal feedback efficiency  $\epsilon_{\text{f,high}} = 0.1$ ) of the radiated luminosity is deposited in the gas as thermal energy. At low Eddington ratios ( $\eta < \eta_{\text{crit}}$ ), kinetic energy is injected by kicking particles along randomly chosen directions at irregular time intervals. As we shall see later, in our simulations, the high- $z$  BH accretion is strongly regulated by thermal feedback, with kinetic feedback playing a negligible role.

We consider four distinct BH accretion models. The first two follow Eddington-limited accretion, differing in their adopted radiative efficiencies and boost factors. The first model uses the same parameters as the TNG simulations—specifically,  $\epsilon_r = 0.2$ ,  $\alpha = 1$ ,  $f_{\text{edd}} = 1$ —and is referred to as the “TNG accretion model.” The second adopts a lower radiative efficiency and a higher boost factor, i.e.,  $\epsilon_r = 0.1$ ,  $\alpha = 100$ ,  $f_{\text{edd}} = 1$ . We refer to this as the “TNG-BOOST” accretion model. We note here that while TNG-BOOST changes both  $\alpha$  and  $\epsilon_r$  compared to TNG, we show in Appendix B that  $\epsilon_r$  has a much stronger impact than  $\alpha$ . To explore the impact of super-Eddington growth, we also implement two additional models that allow for accretion up to ten times the Eddington rate ( $f_{\text{edd}} = 10$ ), while keeping the radiative efficiency and boost factor the same as in the TNG and TNG-BOOST models. These are labeled “TNG-SE” ( $\epsilon_r = 0.2$ ,  $\alpha = 1$ ,  $f_{\text{edd}} = 10$ ) and “TNG-BOOST-SE” ( $\epsilon_r = 0.1$ ,  $\alpha = 100$ ,  $f_{\text{edd}} = 10$ ), respectively.

We acknowledge that our modeling of the super-Eddington phase is simplistic, as we do not account for the expected reduction in radiative efficiency due to photon trapping and advection in this regime (Jiang et al. 2019; Massonneau et al. 2023). As a result, we are likely to overestimate the AGN feedback received by the host galaxy during this phase. Detailed modeling of super-Eddington accretion, such as that presented in Lupi (2024), is beyond the scope of this paper and is reserved for future work. Here, we simply modify (in post-processing) the bolometric luminosity calculation

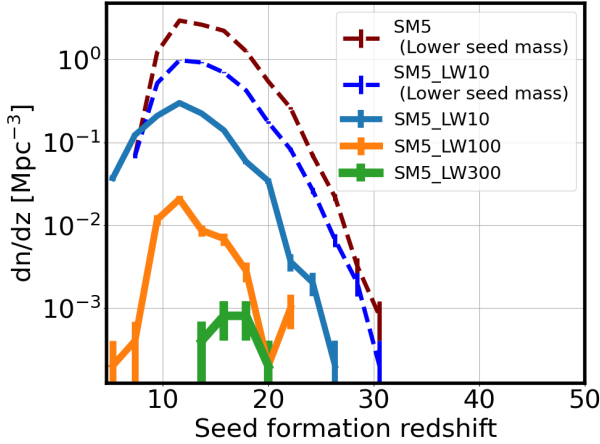


**Figure 3.** Predicted number density of new BH seeds per unit redshift ( $dn/dz$ ) for the various seed models explored in this work. All solid lines correspond to a fiducial seed mass of  $M_{\text{seed}} = 1.5 \times 10^5 M_{\odot}$ , which produce peak seeding abundances ranging from  $\sim 10^{-3} - 0.3 \text{ Mpc}^{-3}$  per unit redshift depending on the critical LW flux. The dashed lines correspond to the two higher-resolution supplementary runs that assume  $M_{\text{seed}} = 1.8 \times 10^4 M_{\odot}$ , predicting peak seed abundances of  $\sim 0.8$  &  $5 \text{ Mpc}^{-3}$ .

in the super-Eddington phase by adopting a logarithmic scaling with the black hole accretion rate (as in Volonteri et al. 2015), given by  $L_{\text{bol}} = L_{\text{Edd}} (1 + \ln f_{\text{Edd}})$  where  $L_{\text{Edd}} = \epsilon_r M_{\text{Edd}} c^2$ .

### 2.3. Black hole seeding

We use the gas-based heavy seed models developed in Bhowmick et al. (2021) and Bhowmick et al. (2022a). Seeds are formed in sufficiently resolved halos ( $> 32$  DM particles) based on the following seeding criteria:

- *Dense & metal poor gas mass criterion:* Seeds are placed inside halos that exceed a critical mass threshold of gas that is denser than the star formation threshold ( $\geq 0.13 \text{ cm}^{-3}$ ) while also being metal-poor ( $\leq 10^{-4} M_{\odot}$ ). This threshold is prescribed in the units of  $M_{\text{seed}}$  and is denoted by  $\tilde{M}_{\text{sfmp}}$ . While a wide range of thresholds have been explored in our previous papers (Bellovary et al. 2021; Bhowmick et al. 2024b), here we adopt  $\tilde{M}_{\text{sfmp}} = 5$ .
- *LW flux criterion:* We require the dense and metal poor gas mass to also be exposed to a minimum amount of LW flux ( $J_{\text{crit}}$ ). Since our simulations do not include direct radiative transfer, the LW flux is computed from nearby star forming regions based on the analytical formalism of Dijkstra et al. 2014 (see Bhowmick et al. 2022a for more details). Star formation is suppressed within the seed form-

ing gas despite the densities exceeding the star formation threshold. We have explored three values of critical LW fluxes, namely 10, 100 & 300  $J_{21}$ .

- *Halo mass criterion:* Our mass resolution naturally sets a minimum mass threshold above which seeds are allowed to form. We assign a minimum count of  $> 32$  DM particles for an FOF to be called a “halo”. This implies a minimum mass threshold of  $6.1 \times 10^7 M_{\odot}$  for our default resolution simulations, and  $7.6 \times 10^6 M_{\odot}$  for higher resolution simulations.

We explore the following seed model variations in our runs: At our default resolution ( $N_{\text{dm}} = 360^3$ ), we adopt a seed mass of  $M_{\text{seed}} = 1.5 \times 10^5 M_{\odot}$ , which is approximately the gas mass resolution. We then run simulations that apply all of the above criteria and explore the impact of varying  $J_{\text{crit}}$ . These are denoted by **SM5\_LW10** ( $\tilde{M}_{\text{sfmp}}, J_{\text{crit}} = 5, 10$ ), **SM5\_LW100** ( $\tilde{M}_{\text{sfmp}}, J_{\text{crit}} = 5, 100$ ), and **SM5\_LW300** ( $\tilde{M}_{\text{sfmp}}, J_{\text{crit}} = 5, 300$ ). To test the impact of the seed mass, we ran two higher-resolution simulations (with  $N_{\text{dm}} = 720^3$ ), adopting a lower seed mass of  $M_{\text{seed}} = 1.8 \times 10^4 M_{\odot}$ . One of these used the **SM5\_LW10** model, while the other applied only the *dense and metal-poor gas mass criterion*, and is referred to as **SM5**. For the **SM5\_LW10** model, we run simulations that explore variations of BH dynamics, accretion, AGN feedback, stellar feedback, as detailed in Section 2.5.

Finally, we ran two additional simulations to test the sensitivity of our results to box size and resolution (see Appendix A). Both adopt the **SM5\_LW10** seeding model with  $M_{\text{seed}} = 1.5 \times 10^5 M_{\odot}$ . One uses the default mass resolution but an eight-times larger volume; the other uses the default volume but an eight-times higher mass resolution.

Figure 3 shows the overall abundance of BH seeds produced by the various seed models in our 5SIGMA\_COMPACT constrained boxes. Depending on the model, the onset of seed formation occurs between  $z \sim 15-30$ , with peak seed formation occurring between  $z \sim 9-17$ . At lower redshifts, seed formation is suppressed due to metal enrichment and the decreasing gas content in halos, driven by stellar feedback. This of course occurs for our models by construction, given our threshold constraints. For models with  $\sim 10^5 M_{\odot}$  seeds, the most lenient model, **SM5\_LW10**, produces peak seed abundances of  $\sim 0.3 \text{ Mpc}^{-3}$  per unit redshift. In contrast, the most restrictive model, **SM5\_LW300**, yields seed abundances no higher than  $\sim 10^{-3} \text{ Mpc}^{-3}$ , broadly consistent with the predictions of O’Brennan et al. (2025). For the supplementary high-resolution boxes with lower-

mass ( $\sim 10^4 M_\odot$ ) seeds, the peak seed abundances reach  $\sim 0.8 \text{ Mpc}^{-3}$  and  $\sim 5 \text{ Mpc}^{-3}$  for the SM5\_LW10 and SM5 models, respectively. Our seed models influence the final fate of BHs at  $z \sim 6-10$  in two key ways: first, they affect the timing of seed formation, providing more time for early-forming seeds to grow via gas accretion and second, a greater abundance of progenitor halos (of the target  $3 \times 10^{12} M_\odot$  halo at  $z = 6$ ) forming seeds can enhance BH growth through mergers.

The above seed models have been explored in our previous studies (Bhowmick et al. 2021, 2024b) within uniform and zoom simulation setups. Many of these models have been shown to broadly reproduce the current abundances and mass estimates of the JWST BHs at  $z \sim 4-6$  (Bhowmick et al. 2024c) as well as the local BH populations (Bhowmick et al. 2025a). The results of this work could be used to assess the implications of the “ultra-high” redshift ( $z \sim 9-11$ ) JWST BHs as well as the high-z ( $z \sim 6$ ) quasars simultaneously.

#### 2.4. Black hole dynamics and mergers

Nearly all of our simulations trace BH dynamics that determines mergers using a subgrid dynamical friction (DF) model. This subgrid-DF model accounts for the missing dynamical friction force due to insufficient spatial and mass resolution. Specifically, we use the Ma et al. (2023) model that adds the following correction to the BH accelerations:

$$\mathbf{a}_{\text{df}} = \sum_i \frac{\alpha_i b_i}{(1 + \alpha_i^2)(r_i + r_{\text{soft}})} \left( \frac{G\Delta m_i}{(r_i + r_{\text{soft}})^2} \right) \hat{\mathbf{V}}_i. \quad (4)$$

with  $\alpha_i \approx b_i V_i^2 / GM_{bh}$  and  $b_i \equiv r_i \left| \hat{\mathbf{r}}_i - (\hat{\mathbf{r}}_i \cdot \hat{\mathbf{V}}_i) \hat{\mathbf{V}}_i \right|$ . The summation is performed over all the mass resolution elements that the code encounters on the PM tree during the usual gravity calculation.  $\Delta m_i$ ,  $\mathbf{r}_i$ , and  $\mathbf{V}_i$  are the mass, relative displacements and relative velocities of each resolution element with respect to the BH.  $r_{\text{soft}}$  is softening length for a given particle type. Additionally, since the dark matter (DM) particle mass is  $\sim 10$  times larger than the seed mass, we initialize BH seeds with an enhanced *dynamical seed mass* of  $24 M_{\text{seed}}$  ( $\sim 2.4 M_{\text{DM}}$ ). This is done to mitigate spurious numerical heating of the seeds caused by interactions with the more massive background DM particles. Although the *true* BH mass used in the seeding, accretion and feedback routines is set to the actual seed mass ( $M_{\text{seed}}$ ), the *dynamical* seed mass determines the *gravitational* mass used for computing BH accelerations.

We merge two close BHs when they are gravitationally bound, with separations within two times the gravitational softening length of DM (i.e. 1.46 kpc). For gravitational boundedness, we require  $|\Delta\mathbf{v}|^2/2 + \Delta\mathbf{a} \cdot \Delta\mathbf{r} <$

$\mathbf{0}$  where  $\Delta\mathbf{v}$ ,  $\Delta\mathbf{a}$  and  $\Delta\mathbf{r}$  are the relative velocities, relative accelerations and relative displacement between the BH pairs. We extensively explored the above dynamics setup (along with model variations) with our gas-based seed models in Bhowmick et al. (2025b) that focused on lower-mass  $\sim 10^3 M_\odot$  seeds. In this work, we apply this dynamical model to the vast majority of our simulations to understand the growth of heavy seeds and the implications of  $z \sim 6$  quasars and  $z \sim 9-11$  JWST AGN.

Finally, we also ran a simulation that employs the widely used technique of pinning, or “repositioning,” BHs to the local potential minima at every time-step. As mentioned previously, this BH repositioning scheme has been employed in many previous hydrodynamic simulations (Khandai et al. 2015; Feng et al. 2016; Nelson et al. 2019; Bhowmick et al. 2024b,c, 2025a). In contrast to simulations that use subgrid-DF, repositioning ensures that BHs merge instantaneously during galaxy mergers. Therefore, comparing results from the repositioning and subgrid DF models allows us to assess the overall efficiency of BH mergers and the downstream impact of these assumptions on the BH merger rates.

#### 2.5. Summary of the simulation suite

Our simulation suite primarily consists of  $[13.3 \text{ Mpc}]^3$  constrained simulation boxes that produce a  $3 \times 10^{12} M_\odot$  halo by  $z = 6$ . In these boxes, we systematically vary our prescriptions of BH seeding, dynamics, accretion, AGN feedback and stellar feedback. Based on these variations, we can envision our simulation suite as composed of three parts:

- The first part is designed to isolate and distinguish between the impact of BH seeding and accretion. Therefore, all the boxes here use the 5SIGMA\_COMPACT IC and adopt a fixed prescription for BH dynamics (subgrid-DF), as well as AGN and stellar feedback (inherited from `IllustrisTNG`). At the default resolution with  $M_{\text{seed}} = 1.5 \times 10^5 M_\odot$ , we run boxes with variations among three seed models—SM5\_LW10, SM5\_LW100, and SM5\_LW300, coupled with the four different accretion models: TNG, TNG-SE, TNG-BOOST, and TNG-BOOST-SE. This amounts to  $3 \times 4 = 12$  default resolution simulations. We additionally run two higher-resolution boxes (SM5 and SM5\_LW10) with a lower seed mass of  $M_{\text{seed}} = 1.8 \times 10^4 M_\odot$ .
- The second part is designed to isolate the impact of BH dynamics, stellar feedback and AGN feedback. Here we took the most lenient seeding and

accretion model, and ran three additional simulations using the `5SIGMA_COMPACT` IC. Each varies only one component relative to the main simulation suite: the first replaces our subgrid DF dynamics model with BH repositioning; the second retains the subgrid DF model but disables stellar feedback; and the third reduces the AGN thermal feedback efficiency to  $\epsilon_{\text{f,high}} = 0.001$  (100 times smaller than TNG).

- The third part consists of a few supplementary boxes to isolate the impact of resolution, volume and environment. All of these use the most lenient seeding and accretion model. The first box uses the default resolution with  $8\times$  larger volume ( $[26.6 \text{ Mpc}]^3$ ); the second box uses the default volume at  $8\times$  higher mass resolution ( $N_{\text{dm}} = 720^3$ ). The third box uses the default volume and resolution, but with the `5_SIGMA_TYPICAL` IC.

### 3. RESULTS

We now examine how our BH seeding, dynamics, accretion and feedback models influence the evolution of BHs and their accompanying host galaxies. In Figure 4, we present results from our main simulation suite, showing the evolution of the most massive BH in our most massive halo across different snapshots for our various seeding and accretion models. The panels display the evolution of BH mass<sup>1</sup> (top row), stellar mass (middle row), and the BH-to-stellar mass ratio (bottom row). We also include various observed high-redshift BH populations. The  $z \sim 6-7$  quasars span a range of BH masses beginning at  $\sim 10^7 M_{\odot}$  (plotted as grey circles), but here we focus on the most luminous systems, which host BHs with masses  $\gtrsim 10^9 M_{\odot}$  (black horizontal line). For a subset of these quasars, we also show the host galaxy stellar mass (black pentagons) measurements that have been enabled by recent JWST follow-up observations (Onoue et al. 2024; Ding et al. 2025). Lastly, we highlight the JWST-detected BHs at  $z \sim 9-11$ : CEERS-1019 (circle), GN-z11 (square), UHZ1 (triangle), GHZ9 (star) and CAPERS-LRD-z9. While these observations hold the potential to place strong constraints on BH seeding and growth models, we are still at the very early stages of probing BH populations at such high redshifts. At present, only a handful of BHs have been detected, and our constrained simulations similarly cannot capture the

full diversity of environments in which these objects may form and evolve. As such, neither current simulations nor observations yet provide statistically robust constraints. Moreover, the quoted BH mass estimates for these systems carry significant statistical and systematic uncertainties, as discussed in Section 4.5. Nonetheless, we compare our simulations with the available observations, illustrating their potential to meaningfully constrain models in the future.

#### 3.1. *Mergers vs accretion dominated BH growth*

For the BH mass assembly (top row of Figure 4), the first thing to note is the relative contribution of BH accretion versus BH–BH mergers, as seen by comparing solid and dashed lines of the same color. The evolution of BH mass exhibits two distinct regimes: a merger-dominated phase at  $z \gtrsim 9$  and an accretion-dominated phase at  $z \lesssim 9$ . While we identified these regimes in B22, there we used BH repositioning which tends to overestimate merger rates. Here we demonstrate that even with subgrid-DF, these two regimes persist. This is most clearly visible in the most permissive seeding model, `SM5_LW10`, which yields a higher number of mergers. However, the efficiency of BH–BH mergers is dramatically reduced in the absence of repositioning (discussed in more detail later in the next subsection).

Crucially, even when BH mergers are completely eliminated – as occurs in the most restrictive seeding model ( $J_{\text{crit}} = 300 J_{21}$ ) – gas accretion alone does not significantly increase the mass of BH above the seed value until after  $z \sim 9$ . As we shall see in Section 3.4, this suppression of gas accretion is caused by the combined impact of stellar and AGN feedback. As a result, in our simulations, substantial BH growth at  $z \gtrsim 9$  requires BH–BH mergers.

A notable imprint of the transition between merger-dominated and accretion-dominated BH growth can also be seen in the evolution of the stellar mass to BH mass ratio ( $M_{\text{bh}}/M_{*}$ , bottom row of Figure 4). More specifically, in the merger-dominated regime at  $z \gtrsim 9$ ,  $M_{\text{bh}}/M_{*}$  decreases with time, that is, galaxies grow faster than BHs. This is not surprising, as the BHs grow primarily via mergers, while the galaxies grow through both mergers and in-situ star formation. In contrast, when gas accretion dominates BH growth at  $z \lesssim 9$ ,  $M_{\text{bh}}/M_{*}$  increases with time down to  $z \sim 6$  for the vast majority of our seed models. In general, the different regimes of merger-dominated growth (at  $z \gtrsim 9$ ) and accretion-dominated growth (at  $z \lesssim 9$ ) have significant implications for how our seeding, accretion, and dynamics models influence the assembly of the BH mass.

<sup>1</sup> Note that while the mass of the central BH in the most massive halo generally increases with decreasing redshift, occasional decreases do occur. This is simply due to the most massive halo being intermittently reassigned to a different halo with a lower central BH mass.

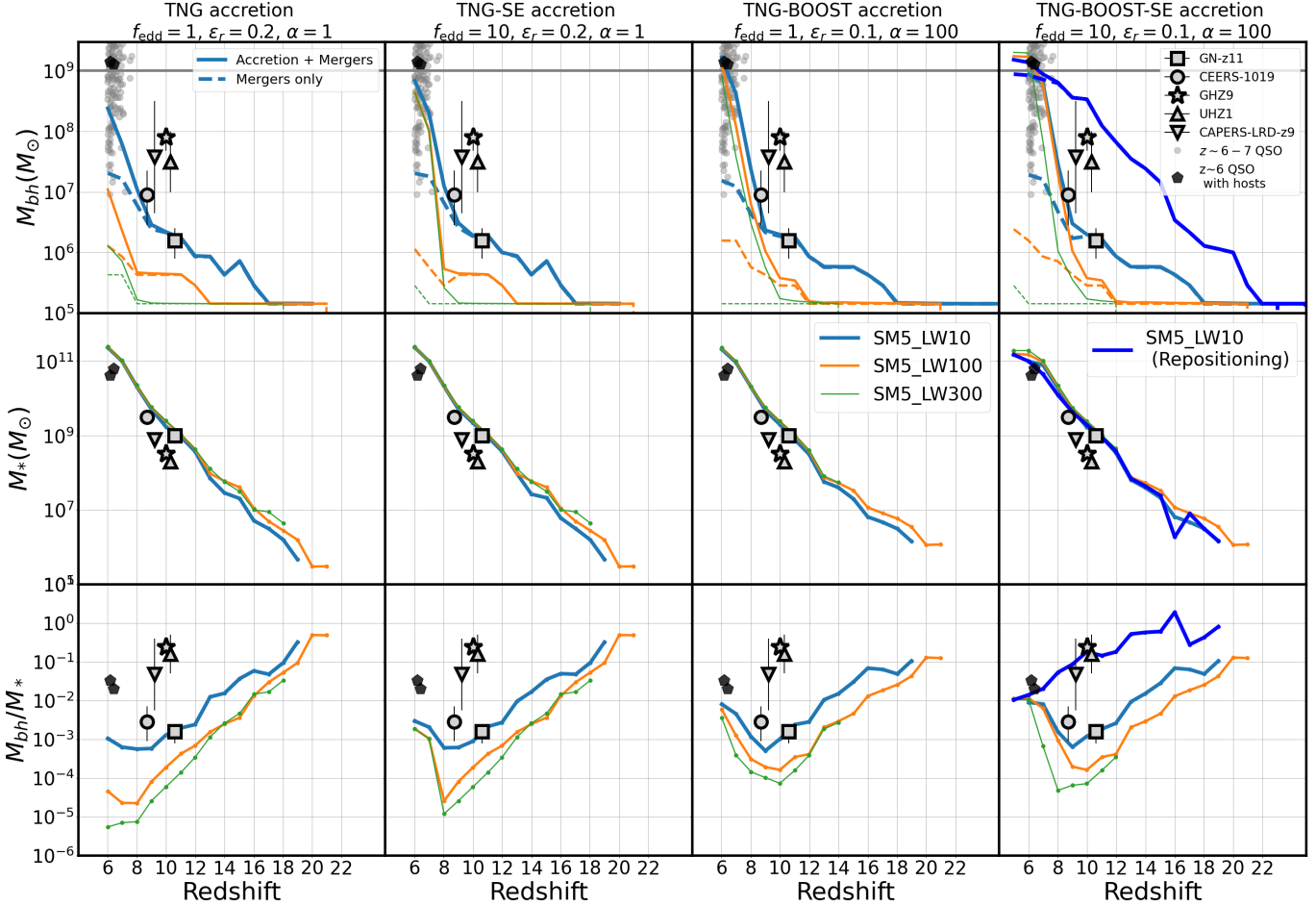


**Figure 4. BH mass assembly for different seeding and accretion models:** Evolution of the most massive BH in the most massive halo across redshift snapshots. The top row shows the BH mass ( $M_{bh}$ ), where the solid line denotes the total BH mass growth (from both accretion and mergers), while dashed lines indicate the contribution from mergers alone. The middle and bottom rows display the stellar mass ( $M_*$ ) and the  $M_{bh}/M_*$  ratios, respectively. The blue, orange, and green curves in each panel represent the three seed models with our default seed mass of  $1.5 \times 10^5 M_\odot$ , corresponding to  $J_{\text{crit}} = 10, 100, \& 300 J_{21}$ . The four columns correspond to the four different accretion models. In the last column, we show an additional simulation with  $J_{\text{crit}} = 10$  that uses BH repositioning instead of subgrid-DF (dark blue line). Faded grey circles mark observed  $z \gtrsim 6$  quasars, while dark pentagons highlight the subset with host galaxy mass measurements. The horizontal line indicates  $10^9 M_\odot$ , which we adopt as the minimum threshold for claiming that a simulation has successfully produced a  $z \sim 6$  quasar. The larger circle, square, triangles, and star correspond to the  $z \sim 9-11$  JWST AGN (see legend). BH growth is dominated by mergers at  $z \gtrsim 9$  and by gas accretion at  $z \lesssim 9$ . As a result, a lenient accretion model significantly enhances the BH mass assembly at  $z \lesssim 9$ , but has a negligible impact on the BH growth at  $z \gtrsim 9$ . On the other hand, changing the seed model has the strongest impact at  $z \gtrsim 9$  as it determines the number of seeds that are available to fuel BH-BH mergers.

### 3.2. Impact of seeding and dynamics modeling

Figure 4 clearly shows that different seed models lead to substantial differences in BH mass assembly. The strongest differences appear in  $z \gtrsim 9$ , mainly due to the natural suppression of merger-driven growth as seed models become more restrictive. Only the most lenient seed model ( $J_{\text{crit}} = 10 J_{21}$ ) is capable of growing  $\sim 10^6-10^7 M_\odot$  BHs from  $\sim 10^5 M_\odot$  seeds by  $z \sim 9-11$ , consistent with the observed BH masses in CEERS-1019 and GN-z11. The BH mass in a source like GN-z11 would be assembled almost entirely through BH-BH

mergers, while that of CEERS-1019's mass requires a combination of mergers and gas accretion. Additionally, the host stellar masses and  $M_{bh}/M_*$  ratios predicted by this seeding model are also close to those observed in both objects. In contrast, the more restrictive seed models with  $J_{\text{crit}} = 100$  and  $300 J_{21}$  fail to reproduce the measured BH masses in GN-z11 and CEERS-1019 range due to an insufficient number of available seeds to drive significant merger-driven growth.

To assess the impact of our BH dynamics implementation (via subgrid-DF) on BH growth, we re-ran our most

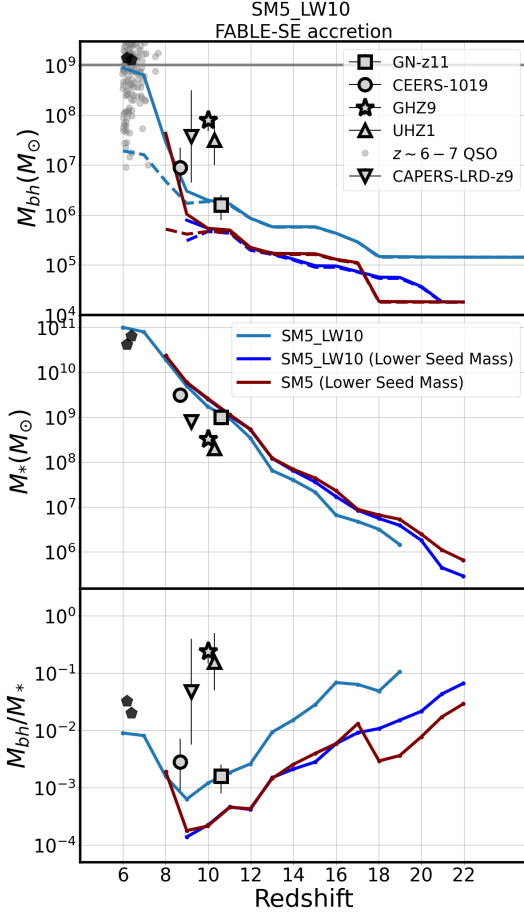


**Figure 5.** Similar to the previous figure, but here we compare the main simulations with the default seed mass ( $1.5 \times 10^5 M_{\odot}$ ), against the supplementary simulations with the lower seed mass ( $1.8 \times 10^4 M_{\odot}$ ). All the lines assume the most lenient seeding ( $J_{\text{crit}} = 10 J_{21}$ ) and accretion (TNG-BOOST-SE) model. Despite the lower seed masses forming at 4 & 10 times higher abundances (revisit Figure 3), they cannot merge efficiently due to weaker dynamical friction. As a result, they produce  $\sim 6$  times smaller BH masses at  $z \sim 10$ .

lenient seed model (blue line in the rightmost column of Figure 4) using BH repositioning. This prescription ensures that BHs promptly merge whenever their host galaxies merge. Repositioning leads to dramatically enhanced merger-driven BH growth, yielding much larger BH masses at  $z \gtrsim 9$ , where mergers dominate BH assembly. In the SM5\_LW10 model, the most massive BHs reach  $\sim 3 \times 10^8 M_{\odot}$  by  $z \sim 10$ , nearly two orders of magnitude higher than with subgrid-DF. Overall, this demonstrates that including subgrid-DF substantially reduces BH merging efficiency, thereby significantly suppressing early merger-driven BH growth. As a result, none of the subgrid-DF based simulations come remotely close to assembling BHs with the measured masses of UHZ1

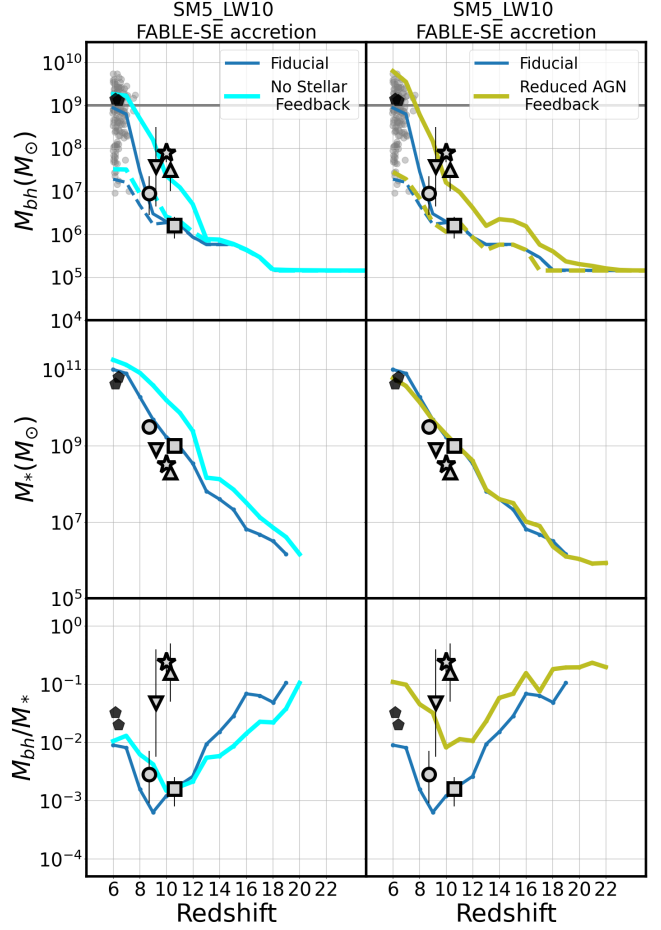


**Figure 6.** Here we show the impact of stellar feedback and AGN feedback on the BH assembly history using simulations with a fixed seed model (SM5\_LW10) and accretion model (TNG-BOOST-SE). The blue line corresponds to the default feedback models inherited from IllustrisTNG. The cyan line keeps the default AGN feedback but removes stellar winds. The green line keeps the default stellar feedback model but reduces the AGN thermal feedback efficiency by a factor of 100. Both of these enhance accretion significantly, causing the onset of gas accretion to occur at earlier times compared to the default setup.

and GHZ9 ( $\sim 10^7$ – $10^8 M_{\odot}$ ) at  $z \sim 9$ . This is despite the fact that our 5SIGMA\_COMPACT simulations produce stellar masses that are  $\sim 5$  times higher than those of the observed host galaxies of UHZ1 and GHZ9. In fact, these objects have the highest  $M_{\text{bh}}/M_{\ast}$  ratios discovered so far. In the absence of significant BH accretion, the only way to increase the  $M_{\text{bh}}/M_{\ast}$  ratios is by enhancing the merging efficiencies at high  $z$ . Under repositioning, the SM5\_LW10 seed model produces a  $M_{\text{bh}}/M_{\ast}$  of  $\sim 0.2$  at  $z \sim 9$ , comparable to the current estimates for  $M_{\text{bh}}/M_{\ast}$ . While the repositioning model produces unrealistically optimistic BH merging efficiencies, at the very least, it indicates that these ratios could be repro-

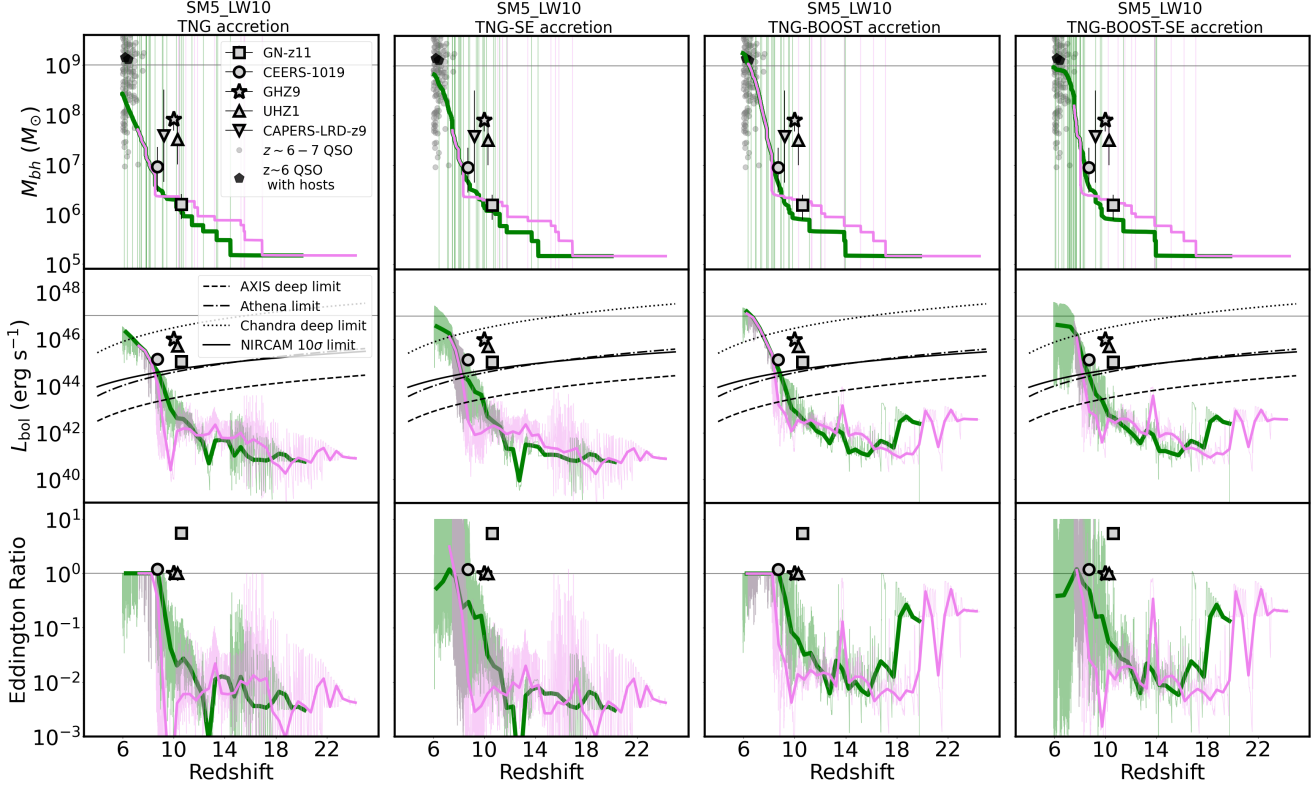


**Figure 7.** For the most lenient seed model (with  $M_{\text{seed}} = 1.5 \times 10^5 M_{\odot}$ ), we select the most massive  $z = 6$  BH and trace the evolution history of BH mass, bolometric luminosity, and Eddington ratio from top to bottom panels, at the actual time resolution of the simulation (much higher than the snapshot resolution). Left to right columns go from the most restrictive to the most lenient accretion model. Two massive, rapidly growing progenitors—shown in green and pink—merge at  $z \sim 7.5$ . Vertical lines on the top panels indicate the redshifts of all mergers involving these progenitors. In the middle panels, the thick line shows the median luminosity over redshift intervals of  $\Delta z = 0.5$ , whereas the thin lines show luminosity variations at the actual time resolution. We also show the detection limits of JWST-NIRCam, Athena, *AXIS*, and *Chandra* (0.5–3 keV band), derived using bolometric corrections from Shen et al. (2020). The 0.5–3 keV X-ray flux limits for Athena and *AXIS* are assumed to be  $2 \times 10^{-17}$  and  $2 \times 10^{-18}$  erg cm $^{-2}$  s $^{-1}$ , respectively, based on Figure 5 of Mushotzky et al. (2019). The horizontal black line marks  $10^{47}$  erg s $^{-1}$ , which we assume to be the target  $z \sim 6$  quasar luminosity for our simulations. Except for the TNG accretion model, all the accretion models achieve that luminosity at  $z \sim 6$ . The CEERS-1019 luminosity mildly favors the TNG-BOOST-SE and TNG-SE accretion model. GN-z11 luminosity cannot be reproduced by any of our models, with only the most lenient TNG-BOOST-SE accretion model coming marginally close.

duced by our lenient seed models if the merging time-scales were significantly shorter than predicted by our subgrid-DF model.

The combined impact of seeding and dynamics is further illustrated by the higher-resolution simulations with lower-mass  $\sim 10^4 M_{\odot}$  seeds (Figure 5). Here we examine its impact on the merger-driven growth at  $z \gtrsim 9$  under our most lenient seed models. In fact, in one of these boxes, we also removed the *LW flux criterion*, allowing  $\sim 10^4 M_{\odot}$  seeds to form in any halo hosting dense, pristine, star-forming gas—a scenario potentially more representative of the NSC seeding channel. Although this produces  $\sim 5$ – $10$  times more  $\sim 10^4 M_{\odot}$  seeds compared to the most lenient model with  $\sim 10^5 M_{\odot}$  seeds, the total BH mass at  $z \sim 9$  is  $\sim 6$  times smaller (blue and maroon lines). Consequently, these lighter seed models

fail to assemble the measured mass of GNz-11, and only marginally reach the measured CEERS-1019 mass. This is primarily because the merging efficiency of  $\sim 10^4 M_{\odot}$  seeds is significantly lower than that of  $\sim 10^5 M_{\odot}$  seeds, owing to weaker dynamical friction. Taken together, these results suggest that assembling BH masses comparable to GNz-11 and CEERS-1019 requires not only efficient heavy seed formation, but also seed masses at the uppermost end of the heavy seed distribution, i.e., around  $\sim 10^5 M_{\odot}$ .

### 3.3. Impact of accretion modeling

Since accretion is suppressed at  $z \gtrsim 9$ , the choice of our accretion model does not have a significant consequence on BH growth in this regime. But at  $z \lesssim 9$ , the accretion model naturally has a much more dramatic

impact on the BH mass assembly. The most restrictive TNG accretion model produces the  $z \sim 6$  BH masses that are  $\sim 10^6$ ,  $10^7$ , and  $2 \times 10^8 M_\odot$  for  $J_{\text{crit}} = 10, 100$ , and  $300 J_{21}$ , respectively. Under this accretion model, we fail to reproduce the  $\gtrsim 10^9 M_\odot$  BHs that power the brightest  $z \sim 6$  quasars for all seed models. When we add super-Eddington accretion (TNG-SE), some of the final  $z \sim 6$  BH masses reach  $\sim 6 \times 10^8 - 8 \times 10^8 M_\odot$  depending on the seed model. This is much closer to the brightest  $z \sim 6$  quasars, albeit slightly lower in mass. For the TNG-BOOST and the TNG-BOOST-SE accretion model,  $\sim 10^9 M_\odot$  BHs are assembled by  $z \sim 6$  for all seed models. Figure 5 further shows that for the TNG-BOOST-SE model,  $\sim 10^4 M_\odot$  seeds are also well on the path toward assembling  $\sim 10^9 M_\odot$  BHs by  $z = 6$  (although we do not run these past  $z = 8$  to save computing resources). These results suggest that the existence of  $\sim 10^9 M_\odot$  BHs within  $z \sim 6$  quasars could provide strong constraints on the accretion model, but not necessarily on seeding models. Unsurprisingly, this is complementary to the implications for the inferred masses of CEERS-1019 and GN-z11 at  $z > 9$  which could provide strong constraints on our seeding models, but not our accretion models. The constraints on seeding are clearly provided by the observed sources that are detected closer to the seeding epoch.

Although at  $z \gtrsim 9$  the assumed accretion models do not affect the BH mass assembly, they naturally impact BH luminosities. In Figure 7, we take the most lenient seed model, and show the evolution of the bolometric luminosity and Eddington ratio for the four accretion models. More specifically, we pick the most massive BH at  $z = 6$ , and trace the evolution of its progenitors. It turns out that this BH has two rapidly growing progenitors that undergo a major merger at  $z \sim 7.5$  when they are both  $\sim 2 \times 10^8 M_\odot$  (shown as green and pink colors). The top panels show that these progenitors have BH masses close to the observed masses for CEERS-1019 and GN-z11. Focusing now on the evolution of luminosity, at  $z \gtrsim 9$ , where the growth of BH is dominated by mergers, the luminosities typically fluctuate between  $\sim 10^{41} - 10^{43} \text{ erg s}^{-1}$ , which is  $\sim 0.1 - 10\%$  of the Eddington limit. At these epochs, the luminosities rarely come close to the Eddington limit. At  $z \lesssim 9$ , when accretion-driven BH growth begins to dominate, there is a steep rise in the luminosities of sources. They now frequently hit the Eddington limit in the TNG and TNG-BOOST models, and exceed it in the TNG-SE and TNG-BOOST-SE models. Note that for TNG-SE and TNG-BOOST-SE, the fluctuations in luminosity are smaller than the Eddington ratio in the super-Eddington regime. This is due to the logarithmic scaling

of the luminosity with the accretion rate in this regime, as discussed at the end of Section 2.2.

At  $z \sim 6$ , except for the TNG model, all the accretion models reach the typical luminosities of  $\sim 10^{47} \text{ erg s}^{-1}$  for the brightest  $z \sim 6$  quasars. For the TNG-BOOST and TNG models, the CEERS-1019 luminosity lies slightly above the peak luminosities around  $z \sim 9$ . For the TNG-BOOST-SE and TNG-SE models, the CEERS-1019 luminosity falls well within the peak luminosities. The GN-z11 luminosity is the hardest to reproduce. For the TNG, TNG-SE and the TNG-BOOST model, the peak luminosities are  $\sim 10$  times lower than that of GN-z11. Only the most permissive TNG-BOOST-SE model produces peak luminosities that are close to (albeit still  $\sim 2 - 3$  times lower than) GN-z11. With that being said, we note that the luminosity fluctuations in our simulations are likely to be underestimated, since we do not resolve the small scale environments (and the fluctuations therein) wherein the actual accretion physics and assumptions matter. However, if we take these luminosities at face value, these results suggest that, unlike the masses, the luminosities of CEERS-1019 and GN-z11 could serve as effective probes for constraining accretion models. In particular, both objects tend to favor models that include super-Eddington accretion, while GN-z11 additionally favors a lower radiative efficiency in combination with a boost in the Bondi accretion rate. Finally, although JWST can detect these sources only near their peak luminosities, future facilities such as *AXIS* should be capable of detecting them over a larger fraction of their duty cycle. However, at much higher redshifts ( $z \gtrsim 12$ ), even instruments like *AXIS* will not be sufficiently sensitive to detect such objects given their predicted luminosities.

Finally, we note that none of our subgrid-DF based simulations are able to reproduce bolometric luminosities as high as those inferred for UHZ1 and GHZ9. This may partly reflect the fact that our simulated  $z \sim 9$  BH masses are significantly lower than the values inferred for these objects. However, under the repositioning scheme, our lenient seed models (SM5\_LW10) can readily assemble  $z \sim 9$  BH masses that can even exceed those of UHZ1 and GHZ9 (right column of Figure 4). It is therefore instructive to examine whether the  $z \sim 9 - 10$  AGN luminosities produced in this scenario are consistent with the observed values. In Figure 8, we show the evolution of mass, luminosity, and Eddington ratio of our most massive BH at high time resolution. Here we also include results from the 5SIGMA\_TYPICAL box because it produces  $z \sim 9 - 10$  stellar masses consistent with the current stellar mass estimates of UHZ1 and GHZ9 (Figure 2, bottom panel). Notably, the  $z \sim 9 - 10$  BH masses produced

in `5SIGMA_TYPICAL` are very close to the observational estimates for these sources. At  $z \sim 10$ , the median luminosity in our simulations is  $\sim 10^{44} \text{ erg s}^{-1}$ , substantially below the observed values for GHZ9 and UHZ1. However, intermittent super-Eddington peaks can reach a few times  $\sim 10^{46} \text{ erg s}^{-1}$ , consistent with the luminosities of both objects. With *JWST*, such sources would be detectable during the bright peaks of their duty cycle, although they remain too faint for *Chandra*. Both these objects were nevertheless detected by *Chandra*—likely due to gravitational lensing by the foreground cluster Abell 2744. A future mission such as *AXIS* would be able to detect these BHs for most of their duty cycle, particularly in the redshift range  $z \sim 10\text{--}12$ . Overall, our repositioning-based simulations can produce not just the currently inferred BH masses of UHZ1 and GHZ9, but also their inferred bolometric luminosities. This implies that the EM detectability of UHZ1 and GHZ9 does not necessarily rule out possibility that their masses assembled primarily via BH mergers. With that being said, the currently inferred bolometric luminosities of these objects may also not be accurate if the bolometric corrections for the high- $z$  Universe turn out to be substantially different compared to standard local AGNs.

### 3.4. Impact of stellar and AGN feedback modeling

Here we explore how the deviations from the default `BRAHMA` implementation of stellar and AGN feedback processes (inherited from `IllustrisTNG`) models impact the accretion-driven BH growth. In Figure 6, we show two additional simulations with our lenient `SM5_LW10` seed model: one with no stellar winds (left panel), and another with AGN thermal feedback efficiency reduced by a factor of 100 (right panel) compared to the fiducial value inherited from `IllustrisTNG`. Not surprisingly, we find that the BH accretion is substantially enhanced in both simulations. In the simulation with no stellar winds, the accretion-driven BH growth starts to become dominant over mergers at much earlier times (at  $z \sim 14$ ) compared to when TNG stellar winds are applied ( $z \sim 10$ ). The resulting BH masses are close to the estimates of UHZ1 and GHZ9. However, reducing stellar feedback also enhances the stellar mass growth (left column, middle low), thereby leaving the  $M_{\text{bh}}/M_{\ast}$  ratios with very little impact. This would make it harder to reproduce the high  $M_{\text{bh}}/M_{\ast}$  ratios currently inferred for UHZ1, GHZ9 and CAPERS-LRD-z9. As mentioned earlier, these high  $M_{\text{bh}}/M_{\ast}$  ratios are much more readily achievable by enhancing the merger-driven BH growth rather than reducing the stellar feedback.

In the simulation with reduced AGN thermal feedback ( $\epsilon_{\text{f,high}} = 0.001$ , which is 100 times smaller than

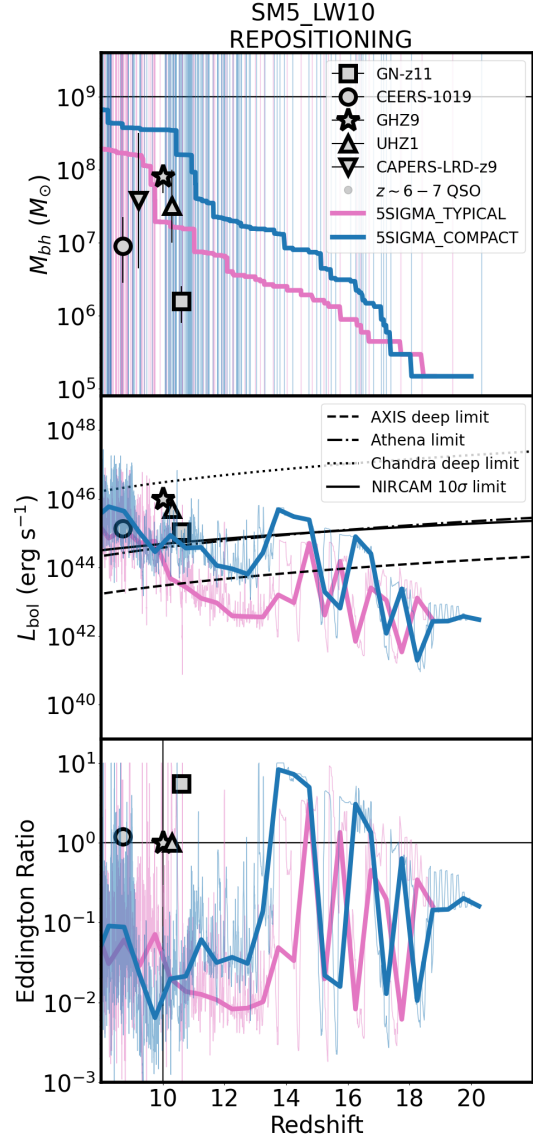


**Figure 8.** High time-resolution evolution of BH mass, bolometric luminosity, and Eddington ratio for the most massive BH at  $z = 8$ , shown for two simulations that employ BH repositioning. The blue and pink lines correspond to the `5SIGMA_COMPACT` and `5SIGMA_TYPICAL` ICs, respectively. The vertical lines in the top panels are BH-BH mergers. The `5SIGMA_TYPICAL` box yields  $z \sim 9\text{--}11$  BH masses comparable to current measurements for UHZ1, GHZ9, and CAPERS-LRD-z9. Notably, this same box also produces stellar masses consistent with those inferred for the hosts of these objects (see Figure 2, bottom panel). Although the BH growth is dominated by mergers, the luminosity—particularly at peak values—remains consistent with the inferred bolometric luminosities of UHZ1 and GHZ9.

TNG), BH accretion is even more substantially enhanced compared to the run without stellar winds<sup>2</sup>. The BH begins to accrete almost immediately after its formation, despite the presence of stellar feedback. This highlights that AGN thermal feedback is likely the dominant mechanism suppressing early BH accretion at high redshift. However, once the AGN feedback becomes sufficiently strong, as in the simulations of TNG and BRAHMA, the stellar feedback further contributes to delaying the onset of accretion-driven BH growth. Notably, reducing AGN feedback can boost BH mass assembly without a corresponding increase in stellar mass, thereby raising the  $M_{\text{bh}}/M_*$  ratio. The resulting BH masses and  $M_{\text{bh}}/M_*$  values are close to the estimates for UHZ1 and GHZ9. These results may point toward a scenario where AGN feedback is intrinsically less efficient at high redshift due to differences in ISM properties and gas conditions, becoming progressively more effective at late times as galaxies evolve. However, this remains an open question that may be investigated using higher resolution simulations with more explicit feedback implementations (e.g. Cho et al. 2024; Guo et al. 2024; Ward et al. 2024; Borodina et al. 2025; Sivasankaran et al. 2025). The gas content and thermal properties of the gas are expected to be vastly different in the very early Universe and hence the dependence of the feedback efficiency with redshift might very well be the kind of physical scenarios that warrant further exploration.

#### 4. DISCUSSION

In this section, we present our results in the context of other works in the literature, discuss potential caveats and limitations in our modeling approach, and the open avenues for future studies.

##### 4.1. High- $z$ quasars and the role of BH accretion

Our constrained simulations show that the choice of the accretion model plays a crucial role in assembling a  $z \sim 6$  quasar. The most restrictive TNG accretion model fails to produce such quasars with any of our seeding models, whereas the more permissive TNG-BOOST and TNG-BOOST-SE accretion models succeed across all seed models. This is consistent with the zoom-in simulations by Bennett et al. (2024), who employed a TNG-BOOST-like accretion within the FABLE galaxy formation model (Henden et al. 2018) and successfully grew a  $\sim 10^9 M_\odot$  BH by  $z \sim 6$ . Our results are also consistent with Huang et al. (2020) and Ni et al. (2022) as

they easily produced these quasars in constrained simulations using the default BlueTides model ( $f_{\text{edd}} = 2$ ,  $\epsilon_r = 0.1$ ,  $\alpha = 100$ ) which is more permissive than our TNG-BOOST accretion model but more conservative than our TNG-BOOST-SE model. Notably, Ni et al. (2022) do not report merger-dominated growth at the earliest times, but that is at least partly because their seeding criterion is much more restrictive than ours.

The superior performance of the TNG-BOOST accretion model relative to TNG in producing  $z \sim 6$  quasars highlights how the lower radiative efficiency can substantially enhance early BH growth. However, the choice of radiative efficiency is uncertain. The standard value of  $\epsilon_r = 0.2$  in the TNG model originates from Illustris (Vogelsberger et al. 2014b) and was motivated by Yu & Tremaine (2002), who inferred such efficiencies for bright, low- $z$  quasars. Whether this assumption applies to quasars at  $z \gtrsim 6$  remains unclear. More recent work by Trakhtenbrot et al. (2017) finds a broader range of radiative efficiencies ( $\sim 0.03$ – $0.3$ ), with a mean around 0.1. Furthermore, Yu & Tremaine (2002) noted that lower-luminosity AGN may have  $\epsilon_r \lesssim 0.1$ , suggesting that assuming a fixed radiative efficiency is likely too simplistic. Complicating matters further, the degeneracy between radiative efficiency and AGN feedback efficiency introduces additional uncertainty into our understanding of quasar growth at high redshift. As we have demonstrated, AGN thermal feedback (as implemented within TNG) is the dominant contributor to the suppression of BH accretion at high- $z$ . Therefore, if the thermal feedback efficiency or the radiative efficiency at high redshift is sufficiently small, it would allow us to produce the  $z \sim 6$  quasars for a much wider range of radiative efficiencies. Additionally, an earlier onset of gas accretion, caused by reduced AGN feedback, could also have significant implications for the JWST-detected AGN and the role of BH-BH mergers discussed in the next subsection.

The above discussion also motivates the exploration of alternative accretion models with weaker dependencies on BH mass, such as the gravitational torque-driven accretion (GTDA) model (Anglés-Alcázar et al. 2017) and the recently proposed free-fall time (FFT)-based accretion model (Weinberger et al. 2025). While the steep  $\dot{M}_{\text{Bondi}} \propto M_{\text{bh}}^2$  scaling of the Bondi prescription can make it disproportionately difficult for lower-mass BHs to grow, we find that this is not a significant bottleneck for the evolution of  $\sim 10^5 M_\odot$  seeds in our simulations. Instead, it is the combination of AGN thermal feedback and stellar feedback that predominantly contributes to suppressing BH accretion at high redshift. Nevertheless, it is important to acknowledge that

<sup>2</sup> We also confirmed using a simulation with no AGN kinetic feedback, that it did not have any influence on the high- $z$  BH accretion.

the Bondi–Hoyle–Lyttleton model relies on idealized assumptions—such as spherical symmetry, negligible angular momentum, and a gravitational potential dominated by the black hole—which are unlikely to hold in realistic galactic or cosmological environments. Accretion models with weaker BH mass scalings may promote more efficient early growth of seed BHs while naturally limiting growth at later times. Furthermore, there may also be a non-linear coupling between the choice of accretion model and AGN feedback, complicating predictions for how early BH growth would differ from that under the Bondi model.

The final consequence of the default TNG-based AGN feedback model is that as we relax the accretion model to enable the assembly of  $z \sim 6$  quasars in our simulations, the choice of seed model has a smaller impact on the final  $z \sim 6$  BH mass (as long as at least one seed is formed). This holds for seed masses in the range of  $\sim 10^4$ – $10^5 M_\odot$ , and is a natural consequence of the self-regulation induced by the AGN feedback. These results are consistent with [Huang et al. \(2020\)](#), who also explored the impact of seeding (albeit with a simple halo mass threshold-based seed model) and found that the seed model was largely inconsequential for high- $z$  quasar assembly in the  $\sim 10^4$ – $10^5 M_\odot$  mass range. However, seeds of lower mass ( $\lesssim 10^3 M_\odot$ ) would still face significant challenges in assembling high- $z$  quasars without substantial super-Eddington growth, as widely acknowledged and also demonstrated in [Natarajan \(2011\)](#); [Huang et al. \(2020\)](#).

#### 4.2. High- $z$ JWST BHs and the role of BH mergers

Due to the combined impact of stellar and AGN feedback in our main simulations, accretion-driven growth becomes significant in our simulations only at  $z \lesssim 9$ . Therefore, unlike for the  $z \sim 6$  quasars, the choice of the accretion model does not play a crucial role in our ability to reproduce the measured masses of the  $z \sim 9$ – $11$  JWST AGNs. As a result, BH mergers play a critical role in assembling the masses of CEERS-1019 and GN-z11 in our simulations. However, semi-analytic models (SAMs) such as the Cosmic Archaeology Tool (CAT; [Trinca et al. 2022, 2024](#)) and A-SLOTH ([Jeon et al. 2025](#)) have successfully reproduced these objects purely through gas accretion ([Schneider et al. 2023](#), see Figures 1 and 2). Furthermore, [Trinca et al. \(2024\)](#) find that the large  $M_{\text{BH}} - M_*$  ratios in these sources can be explained if both light and heavy BH seeds undergo short, repeated episodes of super-Eddington accretion triggered by major galaxy mergers. Similar results are also obtained by [Jeon et al. \(2025\)](#) using the A-SLOTH SAM. With that being said, it is important to note that

the impact of stellar feedback on BH accretion is inherently difficult to capture in SAMs, which do not resolve the internal structure of galaxies. While bursts of super-Eddington accretion do occur in our TNG-SE and TNG-BOOST-SE simulations, they are not strong or persistent enough—likely due to AGN feedback—to drive sufficient BH growth to reach the observed masses of UHZ1 and GHZ9. However, alternative accretion and feedback models may allow for this mode of bursty super-Eddington growth ([Anglés-Alcázar et al. 2015](#); [Weinberger et al. 2025](#)), which we will explore in future work. Interestingly, our results share one key feature with those of [Schneider et al. \(2023\)](#): while their BH masses can be built up via Eddington-limited Bondi accretion, the observed luminosities require short phases of super-Eddington accretion. Similarly, in our simulations, although the BH masses are primarily assembled through BH-BH mergers, the observed luminosities of CEERS-1019 and GN-z11 favor models that include super-Eddington accretion.

Another consequence of the suppressed high-redshift BH accretion, and the central role of mergers in assembling the measured masses of CEERS-1019 and GN-z11, is that our model imposes significantly more stringent requirements on the initial BH seed mass than many previous studies. For example, empirical models employing steady exponential growth of BH can accommodate seed masses as low as  $\sim 100 M_\odot$ , especially if super-Eddington accretion is allowed ([Dayal 2024](#); [Aggarwal 2025](#)). However, again, in our main simulation suite, such rapid BH growth is infeasible at  $z \gtrsim 9$  due to stellar and AGN feedback. Consequently, we must rely on BH-BH mergers to build up the required BH masses. With that being said, even  $\sim 10^4 M_\odot$  seeds have difficulty reaching the observed masses of CEERS-1019 and GN-z11, as dynamical friction is not as effective. Only seeds as massive as  $\sim 10^5 M_\odot$ , if they form in sufficient abundances ( $\sim 0.3 \text{ Mpc}^{-3}$ ), are capable of assembling such objects in our simulations.

To produce enough  $\sim 10^5 M_\odot$  seeds to assemble CEERS-1019- and GN-z11-like BHs, our lenient SM5\_LW10 seeding model assumed that a LW flux of  $10 J_{21}$  is sufficient. However, small-scale radiation hydrodynamic simulations and one-zone chemistry models ([Shang et al. 2010](#); [Sugimura et al. 2014](#); [Regan et al. 2014](#)) indicate that the required fluxes for DCBH formation are significantly higher ( $\gtrsim 1000 J_{21}$ ). Recent work has shown that dynamical heating of gas during major mergers can help relax such stringent flux requirements, though this mechanism typically produces seed masses of only  $\sim 10^3$ – $10^4 M_\odot$  ([Regan et al. 2020b](#); [Prole et al. 2024](#)). These developments highlight the need to explore

additional efficient pathways for forming heavy seeds. For instance, recent high-resolution simulations suggest that some Pop III remnants in these halos may undergo brief hyper-Eddington growth episodes, allowing them to reach the heavy-seed regime (Mehta et al. 2024). Even if only a small fraction of light seeds encounter such favorable conditions, their sheer abundance implies that this channel could substantially enhance the overall number of heavy seeds relative to standard DCBH scenarios. Star-cluster-mediated seed formation scenarios provide another promising avenue. While seeding in NSCs has been extensively explored (Davies et al. 2011; Lupi et al. 2014; Kroupa et al. 2020; Das et al. 2021b,a), the seeding efficiency could be further enhanced if even the off-nuclear clusters could produce heavy seeds. Recently, Dekel et al. (2025) proposed that feedback-free starbursts in the early Universe could generate numerous dense star clusters that can serve as incubators of heavy seeds. This would lead to multiple heavy seeds within the host galaxy, which could then merge and ultimately assemble overmassive BHs. Interestingly, this scenario also invokes merger-driven growth of high- $z$  BHs as found in our simulations, though with a key distinction: in our simulations, mergers occur between BHs seeded in different galaxies, whereas in the Dekel et al. (2025) framework, they arise from seeds formed in separate clusters within a single galaxy.

But even with the most lenient seed models, the estimated BH masses and  $M_{\text{bh}}/M_*$  ratios of UHZ1, GHZ9 and CAPERS-LRD-z9 are challenging to explain, as both merger-driven and accretion-driven black hole growth are too inefficient. These objects have also proven difficult to reproduce through gas accretion in the aforementioned CAT semi-analytic model (see again Figure 2 of Schneider et al. 2023). It is natural to consider that our stellar feedback may be too strong, particularly given the apparent overabundance of bright galaxies in JWST observations compared to most theoretical predictions (Finkelstein et al. 2023). However, when we attempted to enhance BH accretion by reducing stellar feedback, we found that this also increased the stellar mass of the host galaxies, failing to increase the  $M_{\text{bh}}/M_*$  ratios. A more viable pathway is a reduced AGN feedback efficiency at high redshift, as this boosts BH growth in our simulations without significantly affecting stellar mass growth. However, assembling the estimated BH masses of these objects requires the AGN feedback efficiency (or radiative efficiency) to be close to  $\sim 1\%$  of the default TNG values. While such low efficiencies may seem extreme, they may still be possible under special conditions: for instance, super-Eddington accretion with photon trapping in slim disks

can result in lower radiative efficiencies (e.g., Sadowski & Narayan 2016). Furthermore, in dense and clumpy high-redshift environments, AGN radiation could pass through lower-density regions without doing much work on the gas (Ward et al. 2024).

Importantly, Natarajan et al. (2024) reproduced a wide range of observed properties of UHZ1, including not only its luminosity but also the full spectral energy distribution measured by *Chandra* and JWST. Their model invokes a specific direct-collapse scenario: a heavy seed forms in a satellite halo irradiated by a star-forming parent halo that has produced Pop III stars, which supply the Lyman-Werner photons. The two halos then merge, producing an overmassive BH. Notably, even in our simulations, seeds do begin nearly as overmassive as UHZ1 and GHZ9 at  $z \sim 20$  (see middle row of Figure 4). However, our BHs accrete at rates far below Eddington at  $z \gtrsim 10$  because stellar and AGN feedback regulate accretion. As a result, star formation outpaces BH growth, and they do not remain as overmassive by  $z \sim 9\text{--}10$ . By contrast, the empirical modeling of Natarajan et al. (2024) assumes sustained Eddington accretion. This suggests that producing these objects may require even more extreme conditions than those probed by our simulations, where either the initial seed masses are already as massive as  $\gtrsim 10^7 M_\odot$  (Mayer et al. 2024), or stellar and AGN feedback fails to regulate accretion and allow BHs to grow continuously at Eddington rates.

If AGN and stellar feedback indeed suppress and delay high- $z$  BH accretion as strongly as in our main simulations, an alternative avenue is to assume stronger dynamical friction (DF) than what is currently modeled by our subgrid DF implementation (revisit top-right panel of Figure 4). Enhanced DF could accelerate BH mergers and thereby boost merger-driven BH growth without significantly increasing star formation. Notably, Dekel et al. (2025) proposed that a compact stellar galactic disk configuration can significantly increase the dynamical friction and accelerate BH-BH mergers. However, the feasibility of this scenario is yet to be demonstrated in self-consistent numerical simulations. Additionally, a stronger DF may naturally arise in alternative cosmological scenarios, such as self-interacting dark matter (Alonso-Álvarez et al. 2024; Fischer & Sagunski 2024), which we could explore in future work.

Our resolution also poses a significant challenge in modeling the dynamics and eventual mergers of BHs. Although our subgrid-DF model attempts to account for unresolved dynamical friction, the underlying formula of Ma et al. (2023) was derived for softened potentials. By not resolving scattering events on sub-softening scales, we may underestimate dynamical friction and

thus merger-driven BH growth. Moreover, BHs may be embedded in unresolved NSCs, which could further accelerate sinking and mergers (Mukherjee et al. 2024). While our adopted “dynamical” seed mass ( $24 \times M_{\text{seed}}$ ) could mimic the presence of an NSC, the true NSC masses remain uncertain. Conversely, our merger rates may also be overestimated, since we do not explicitly follow the sub-resolution hardening of BH binaries. Processes such as stellar scattering (Merritt 2013), circumbinary disk drag (Siwek et al. 2023, 2024), triple interactions, and gravitational wave (GW) emission are not included, nor do we model GW recoil kicks. Incorporating these mechanisms would likely further suppress the overall merger efficiency. Future work will explore their impact using post-processing prescriptions (Kelley et al. 2017; Sayeb et al. 2021; Satheesh et al. 2025) or on-the-fly implementations (Li et al. 2024; Dong-Páez et al. 2024).

#### 4.3. Suppression of BH accretion by stellar and AGN feedback

The suppression of BH accretion by stellar feedback is a major contributor to why it is significantly more difficult to assemble the estimated masses for the  $z \gtrsim 9$  JWST BHs via accretion in our simulations, compared to SAMs that include AGN self-regulation but neglect the additional impact of stellar feedback. Specifically, due to the delayed onset of accretion, we have to boost BH growth from mergers by using seed models as lenient as  $J_{\text{crit}} = 10 J_{21}$ , to produce the measured masses of CEERS-1019 and GN-z11. In fact, two of the TNG follow-up projects i.e. THE SAN (Kannan et al. 2022) and Millennium-TNG (Pakmor et al. 2023), tend to underpredict the abundances of the  $z \gtrsim 12$  UV luminous galaxies observed by JWST (Kannan et al. 2023). Notably, TNG also has a scaling for enhanced stellar feedback energy at lower metallicities, which leads to stronger feedback at early times. While all this may suggest that TNG stellar feedback is too strong at high- $z$ , it does play a crucial role in reproducing the galaxy stellar mass functions at least up to  $z \sim 10$  (Vogelsberger et al. 2020).

At the other end, the suppression of accretion due to AGN feedback may also be specific to the way it is modelled within `IllustrisTNG`. In particular, the thermal feedback injected on a spherical kernel can readily block the inflow of gas from all directions. However, if the feedback injection is instead modeled as kinetic energy ejected along the polar directions, it could substantially reduce the impact on the gas inflow along the perpendicular plane (Partmann et al. in prep). Finally, even with formal Eddington cap being raised or removed, our

simulations have limited ability to probe the possibility of rapid BH mass assembly via super-Eddington accretion (Schneider et al. 2023; Trinca et al. 2024; Jeon et al. 2025). This is because the formation of extremely dense gas peaks is limited by the resolution as well as the pressurized ISM equation of state. In future work, we plan to address these issues with higher-resolution simulations incorporating more detailed ISM and feedback physics.

Finally, the accretion models employed in the vast majority of cosmological simulations, including `BRAHMA`, do not account for BH spin. However, recent efforts that bridge scales—combining high-resolution GRMHD simulations resolving flows down to the BH horizon with galaxy-scale (kpc) gas dynamics—demonstrate that BH spin plays a critical role in regulating feedback efficiency (Cho et al. 2023, 2024; Su et al. 2025). Incorporating spin dependence may therefore represent a crucial missing ingredient for future models of BH feedback.

With all that being said, the suppression of accretion due to feedback in low mass galaxies has also been seen in other works. This includes not just cosmological simulations (Habouzit et al. 2017; Byrne et al. 2023), but also smaller volume “resolved physics” simulations. Very recently, a series of ultra high resolution ( $\sim 0.5 - 20 M_{\odot}$ ) individual galaxy simulations have illustrated that SNII feedback is primarily responsible for stunting BH accretion in dwarf galaxies (Partmann et al. 2025; Petersson et al. 2025). Furthermore, these papers do not include AGN feedback, which can further suppress BH accretion. In light of these results, primarily merger-driven BH mass assembly for the JWST AGN should not be ruled out. This scenario will be testable with next-generation gravitational wave observatories, particularly the Laser Interferometer Space Antenna (LISA).

#### 4.4. Limitations of constrained ICs

When we simultaneously compare our simulation predictions to  $z \sim 6$  quasar and  $z \sim 9 - 11$  observations, we implicitly assume that the two populations reside in similar environments. At present, there is no strong observational evidence supporting this connection, and previous simulations (Di Matteo et al. 2008) have shown that the most massive BHs at earlier epochs do not necessarily remain the most massive at later times. Nonetheless, both populations represent extreme BH growth scenarios that likely require rare, optimal environments, which our constrained ICs are designed to capture.

At the same time, our constrained simulations fall far short of capturing the full diversity of environments within the cosmic web. In reality, there may well exist regions capable of producing  $z \sim 6$  quasars without forming  $z \sim 9 - 11$  JWST AGNs, and vice versa. Probing

such environments requires simulations spanning much larger cosmological volumes, which is the subject of ongoing work (Zhou et al. in prep). For now, by restricting ourselves to constrained ICs designed to host both populations simultaneously, we are inherently biasing our models toward scenarios where the  $z \sim 9\text{--}11$  JWST AGNs are evolutionary progenitors of the  $z \sim 6$  quasars.

#### 4.5. Observational uncertainties on high- $z$ BHs

A major challenge in constraining BH formation and growth models from current high- $z$  observations is the significant uncertainty in BH mass measurements. For instance, objects like GHZ9 and UHZ1 currently lack direct BH mass measurements; instead, their reported masses are inferred from bolometric luminosities under the assumption of Eddington-limited accretion. As mentioned earlier, these bolometric luminosity estimates themselves are uncertain due to the use of bolometric corrections from low- $z$  AGN that may not be valid at high- $z$ . For CEERS-1019 and GN-z11, more direct BH mass estimates are available via single-epoch virial methods using broad emission lines. However, they are still subject to substantial uncertainty, both from statistical errors in the spectral fitting and systematic uncertainties related to whether the empirically derived low- $z$  relations between the BH masses and broadline widths apply at higher- $z$ . As a result, the error bars on the BH mass estimates may be significantly underestimated. Additionally, several recent works have also suggested that the high- $z$  BH mass measurements may be systematically overestimated (Naidu et al. 2025; Rusakov et al. 2025).

Moreover, at high redshift, stellar masses can be underestimated, especially when derived solely from ultraviolet (UV) luminosity—as was the case for CAPERS-LRD-z9. This is largely due to the ‘outshining’ effect, where recent star formation dominates the UV emission, masking the contribution from older, more massive stars (Narayanan et al. 2024). For spectroscopically confirmed objects, stellar mass estimates from spectral energy distribution (SED) fitting are generally more reliable, though disentangling the AGN and stellar components of the SED remains a challenge (Ramos Padilla et al. 2020).

In summary, both BH and stellar mass measurements for early-universe galaxies are fundamentally limited by observational restrictions and methodological assumptions. However, with improvements in data quality, increased observational volume, and enhanced analysis techniques in the future, we anticipate being able to leverage these observations more effectively to better constrain models of BH formation and growth.

## 5. CONCLUSIONS

In this work, we investigate the assembly of the earliest and most extreme BH populations in rare over-dense environments within the large scale structure. To capture these environments in a small simulation volume of  $[13.3 \text{ Mpc}]^3$ , we use constrained ICs that yield  $\sim 3 \times 10^{12} M_\odot$  halos by  $z = 6$ . These massive high- $z$  halos are considered to be plausible hosts for the brightest  $z \sim 6$  quasars. Additionally, our simulations produce galaxies with stellar masses of  $\sim 10^8\text{--}10^9 M_\odot$  at  $z \sim 9\text{--}11$ , consistent with current estimates for the hosts of the *JWST* AGN. Using the novel seed models developed within the **BRAHMA** simulation framework, together with a subgrid dynamical friction prescription for BH dynamics, we ran a large suite of simulations to systematically explore the impact of seeding, dynamics, accretion, and stellar/AGN feedback modeling on BH. We refer to these runs as the **BRAHMA-CONSTRAINED** simulations.

We place  $\sim 10^4\text{--}10^5 M_\odot$  seeds in halos containing sufficient amount dense, metal-poor gas (at least five times the seed mass) that is also exposed to strong Lyman–Werner (LW) radiation fields (10, 100, and 300  $J_{21}$ ). While the foregoing seed models are motivated from presumed conditions for DCBH seeding, we also run simulations that exclude the LW flux requirement. The subsequent dynamics and merger-driven growth of these seeds are followed using the subgrid DF model from M23. BH growth via gas accretion is modeled using the Bondi–Hoyle formalism, with variations in the maximum Eddington ratio ( $f_{\text{edd}} = 1 \& 10$ ), radiative efficiency ( $\epsilon_r = 0.1 \& 0.2$ ), and the Bondi boost factor ( $\alpha = 1 \& 100$ ).

Under the default stellar and AGN feedback models inherited from **IllustrisTNG**, BH accretion is strongly suppressed at  $z \gtrsim 9$ . Consequently, BH growth at these redshifts is dominated by mergers (provided sufficient seeds form), whereas at  $z \lesssim 9$  it is driven primarily by accretion. This leads to distinct ways in which BH seeding, dynamics, and accretion modeling impact BH growth, which can be summarized as follows:

- BH seed modeling exerts the strongest influence at  $z \gtrsim 9$ , with its impact diminishing at later times, particularly under lenient accretion models. At  $z \sim 9\text{--}10$ , the most permissive model produces  $\sim 10^5 M_\odot$  seeds with abundances of  $\sim 0.3 \text{ Mpc}^{-3}$ . This model assembles BH masses of  $\sim 10^6$  and  $\sim 10^7 M_\odot$  at  $z \sim 10$  and  $z \sim 9$ , respectively, with growth dominated by BH–BH mergers. These masses are consistent with current estimates for GN-z11 and CEERS-1019. By contrast, in the most restrictive seed models, the

few BHs that form barely grow beyond their seed mass by  $z \sim 9$  due to the absence of mergers.

- When the seed mass is lowered to  $\sim 10^4 M_\odot$ , the assembled  $z \sim 10$  BH masses remain  $\lesssim 10^6 M_\odot$  even if they form with  $\sim 10$  times higher seeding abundances compared to the most lenient simulation with  $\sim 10^5 M_\odot$  seeds. This is because the merger-driven growth becomes more inefficient due to weaker dynamical friction.
- Our subgrid DF model yields low BH-BH merger efficiency, producing  $z \sim 9$  BH masses  $\gtrsim 200$  times smaller than simulations that assume prompt BH-BH coalescence after each galaxy merger; consequently, even our lenient seed models cannot assemble  $\gtrsim 10^7 M_\odot$  BHs by  $z \sim 9$ , as currently inferred for UHZ1, GHZ9, and CAPERS-LRD-z9.
- BH accretion modeling strongly impacts BH growth at  $z \lesssim 9$ , but not at earlier times. With sufficiently relaxed accretion parameters that permit super-Eddington growth (e.g.,  $f_{\text{edd}} = 10$ ), or lower radiative efficiency (e.g.,  $\epsilon_r = 0.1$ ), our simulations produce  $\sim 10^9 M_\odot$  BHs powering  $z \sim 6$  quasars, largely independent of the seed model. By contrast, under more restrictive accretion prescriptions, the resulting  $z \sim 6$  BH masses are much smaller, ranging from  $\sim 10^6$ – $10^8 M_\odot$  depending on the seed model.
- While variations in BH seeding, dynamics, and accretion significantly alter BH mass growth, they have negligible impact on the stellar mass assembly of the host galaxies.

Deviations from the standard stellar and AGN feedback models also have a profound impact on BH growth, shifting the boundary between merger- and accretion-dominated regimes, as summarized below:

- The removal of stellar feedback substantially enhances BH accretion, causing accretion-dominated BH growth to begin as early as  $z \sim 14$ . However, it also drives a commensurate increase in stellar mass assembly, leaving the  $M_{\text{bh}}-M_*$  ratios largely unchanged. This makes it difficult to reproduce the high  $M_{\text{bh}}-M_*$  ratios currently inferred for UHZ1, GHZ9, and CAPERS-LRD-z9.
- When AGN thermal feedback is reduced, BH seeds begin accreting immediately upon formation. This results in a dramatic increase in BH mass assembly at earliest stages ( $z \gtrsim 14$ ), while stellar mass assembly remains much less affected. As a consequence, the  $M_{\text{bh}}-M_*$  ratios are significantly enhanced.

Overall, our results demonstrate that different aspects of the physics modeling—BH seeding, dynamics, accretion, and AGN & stellar feedback—have distinct impacts on early BH assembly. Continued observations of the highest- $z$  BHs and galaxies will be crucial for disentangling these effects and constraining BH seeding and growth models. A key step in this direction is to understand the nature of AGN & stellar feedback and how it determines the relative importance of merger- versus accretion-driven BH growth. Under the standard TNG-based feedback implementations, calibrated to reproduce low- $z$  galaxy and BH populations, the strong suppression of accretion at early times implies that reproducing the current BH mass measurements of GN-z11 and CEERS-1019 would require a much more abundant population of the heaviest  $\sim 10^5 M_\odot$  seeds than predicted by direct-collapse models, together with shortened merger timescales to explain the current estimates of UHZ1, GHZ9, and CAPERS-LRD-z9. Alternatively, this tension could be alleviated if AGN feedback were substantially weaker than assumed in TNG. Either outcome highlights the transformative potential of these earliest BH populations in advancing our understanding of BH growth and galaxy formation.

## APPENDIX

### A. IMPACT OF SIMULATION VOLUME AND RESOLUTION

In this section, we test the sensitivity of our results to the choice of simulation volume and resolution for one of our representative setups, the lenient **SM5\_LW10** seed model (with  $M_{\text{seed}} = 1.5 \times 10^5 M_\odot$ ) combined with **TNG-BOOST-SE** accretion. In the left panel of Figure 9, we compare three simulations that are designed to isolate these effects. To assess the impact of resolution, we reran our default volume ( $[13.3 \text{ Mpc}]^3$ ) at 8 times higher mass resolution ( $N_{\text{DM}} = 720^3$ , maroon curves). Finally, to test the effect of volume, we simulated a larger  $[26.6 \text{ Mpc}]^3$  box at the same resolution as our default boxes ( $N_{\text{DM}} = 720^3$ , pink curves). We find that increasing the resolution enhances merger-driven BH growth at early times ( $z \gtrsim 9$ ), primarily due to higher number of BH seeds. The enhancement of seed formation

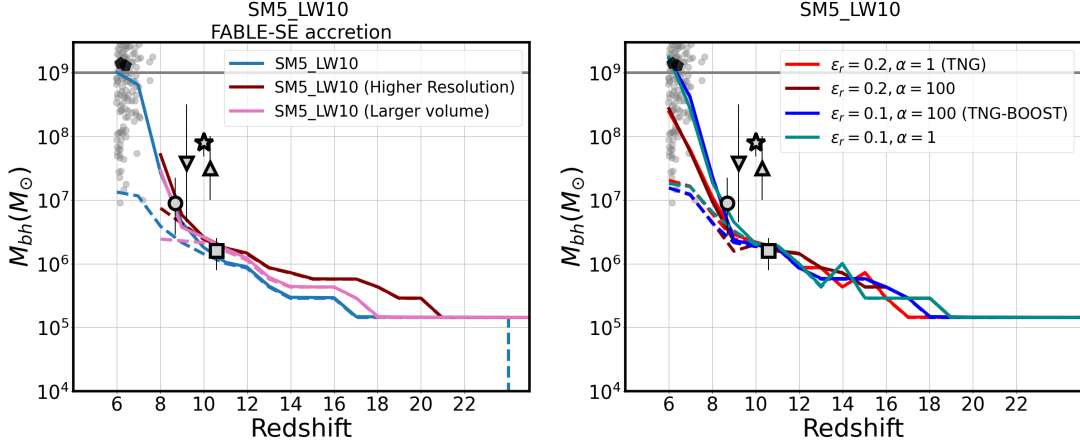


**Figure 9.** *Left Panel:* We test the impact of simulation volume and resolution on the BH growth history for the lenient SM5\_LW10 seed model ( $M_{\text{seed}} = 1.5 \times 10^5 M_{\odot}$ ) combined with TNG-BOOST-SE accretion. The blue curves show our fiducial run ( $[13.3 \text{ Mpc}]^3$  with  $N_{\text{DM}} = 360^3$ ), the maroon curves correspond to the same volume at 8 times higher resolution ( $N_{\text{DM}} = 720^3$ ), and the pink curves correspond to the same resolution but with 8 times larger volume ( $[26.6 \text{ Mpc}]^3$  with  $N_{\text{DM}} = 720^3$ ). At higher resolution, merger-driven BH growth increases due to a larger number of seeds forming as the gas can reach higher densities. A larger volume also mildly enhances growth by producing additional seeds. At  $z \sim 10$ , both higher resolution and larger volume increase the BH mass by factors of  $\lesssim 2$ . Overall, while the effects of resolution and volume are non-negligible, they are not large enough to alter our main conclusions. *Right Panel:* We compare the impact of radiative efficiency ( $\epsilon_r$ ) and Bondi boost factor ( $\alpha$ ) using four simulations with different parameter combinations:  $[\epsilon_r, \alpha] = [0.2, 1]$  (red),  $[0.2, 100]$  (maroon),  $[0.1, 1]$  (lime), and  $[0.1, 100]$  (green). Varying  $\alpha$  has little impact, whereas lowering  $\epsilon_r$  substantially enhances BH growth at  $z < 9$ .

at higher resolutions is simply because it allows for the gas to reach higher densities. We studied this in detail in Bhowmick et al. (2021), which showed that the simulations continue to approach convergence with further increase in resolution. Increasing the simulation volume also leads to a mild increase in merger-driven BH growth. At  $z \sim 10$ , both effects only increase the BH mass by factors  $\lesssim 2$  relative to the default run. At even lower redshifts, the BH masses between all three runs become very similar. Overall, while not negligible, the resolution and volume dependence is not large enough to impact our main conclusions relating to how seeding, dynamics, accretion and feedback modeling influences early BH growth.

## B. IMPACT OF BONDI BOOST FACTOR VS RADIATIVE EFFICIENCY

In the main body of the paper, we showed that switching from the TNG to the TNG-BOOST accretion model leads to a substantial increase in BH mass assembly at  $z < 9$ . However, the transition from TNG ( $[\epsilon_r, \alpha] = [0.2, 1]$ ) to TNG-BOOST ( $[\epsilon_r, \alpha] = [0.1, 100]$ ) simultaneously varies both the Bondi boost factor and the radiative efficiency, making it unclear which parameter drives the difference. In the right panel of Figure 9, we therefore include two additional simulations with  $[\epsilon_r, \alpha] = [0.2, 100]$  and  $[\epsilon_r, \alpha] = [0.1, 1]$ , which allow us to isolate the individual impacts of these parameters. We find that increasing the Bondi boost factor at fixed radiative efficiency has little effect on BH growth, whereas lowering the radiative efficiency significantly enhances BH mass assembly at  $z < 9$ . This is expected, since a lower  $\epsilon_r$  both reduces the injected feedback energy and raises the maximum allowed accretion rate. In contrast, increasing the Bondi boost has only a minor impact, because accretion rates in the TNG model are already close to the Eddington limit at  $z \lesssim 9$  when accretion drives BH growth (see Figure 7). The influence of the boost factor would be stronger in models with a higher ceiling on the accretion rate, although AGN feedback could still impose a limiting effect. In our simulations, however, radiative efficiency is far more consequential for BH mass assembly than the Bondi boost factor.

## ACKNOWLEDGEMENTS

AKB, AMG, and PT acknowledge support from NSF-AST 2346977 and the NSF-Simons AI Institute for Cosmic Origins which is supported by the National Science Foundation under Cooperative Agreement 2421782 and the Simons Foundation award MPS-AI-00010515. AKB and PT also acknowledge support from NSF-AST 2510738. LB acknowledges support from NSF award AST-2307171 and NASA award 80NSSC22K0808. RW acknowledges funding of a Leibniz Junior Research Group (project number J131/2022). LH acknowledges support from the Simons Foundation

under the “Learning the Universe” initiative. The authors acknowledge Research Computing at The University of Virginia and The University of Florida for providing computational resources and technical support that have contributed to the results reported within this publication. URL: <https://rc.virginia.edu>. PN acknowledges support from the Gordon and Betty Moore Foundation and the John Templeton Foundation that fund the Black Hole Initiative (BHI) at Harvard University where she serves as an external PI and NASA HST . The Flatiron Institute is supported by the Simons Foundation.

## DATA AVAILABILITY

The underlying data used in this work shall be made available upon reasonable request to the corresponding author.

## REFERENCES

Agarwal, B., Smith, B., Glover, S., Natarajan, P., & Khochfar, S. 2016, MNRAS, 459, 4209, doi: [10.1093/mnras/stw929](https://doi.org/10.1093/mnras/stw929)

Aggarwal, Y. 2025, MNRAS, 536, 3177, doi: [10.1093/mnras/stae2732](https://doi.org/10.1093/mnras/stae2732)

Akins, H. B., Casey, C. M., Lambrides, E., et al. 2024, arXiv e-prints, arXiv:2406.10341, doi: [10.48550/arXiv.2406.10341](https://doi.org/10.48550/arXiv.2406.10341)

Alexander, T., & Natarajan, P. 2014, Science, 345, 1330, doi: [10.1126/science.1251053](https://doi.org/10.1126/science.1251053)

Alonso-Álvarez, G., Cline, J. M., & Dewar, C. 2024, PhRvL, 133, 021401, doi: [10.1103/PhysRevLett.133.021401](https://doi.org/10.1103/PhysRevLett.133.021401)

Andika, I. T., Jahnke, K., Onoue, M., et al. 2024, A&A, 685, A25, doi: [10.1051/0004-6361/202349025](https://doi.org/10.1051/0004-6361/202349025)

Anglés-Alcázar, D., Davé, R., Faucher-Giguère, C.-A., Özel, F., & Hopkins, P. F. 2017, MNRAS, 464, 2840, doi: [10.1093/mnras/stw2565](https://doi.org/10.1093/mnras/stw2565)

Anglés-Alcázar, D., Özel, F., Davé, R., et al. 2015, ApJ, 800, 127, doi: [10.1088/0004-637X/800/2/127](https://doi.org/10.1088/0004-637X/800/2/127)

Bañados, E., Venemans, B. P., Mazzucchelli, C., et al. 2018, Nature, 553, 473, doi: [10.1038/nature25180](https://doi.org/10.1038/nature25180)

Barnes, J., & Hut, P. 1986, Nature, 324, 446, doi: [10.1038/324446a0](https://doi.org/10.1038/324446a0)

Bañados, E., Venemans, B. P., Decarli, R., et al. 2016, The Astrophysical Journal Supplement Series, 227, 11, doi: [10.3847/0067-0049/227/1/11](https://doi.org/10.3847/0067-0049/227/1/11)

Begelman, M. C., & Silk, J. 2023, MNRAS, 526, L94, doi: [10.1093/mnrasl/slad124](https://doi.org/10.1093/mnrasl/slad124)

Begelman, M. C., Volonteri, M., & Rees, M. J. 2006, MNRAS, 370, 289, doi: [10.1111/j.1365-2966.2006.10467.x](https://doi.org/10.1111/j.1365-2966.2006.10467.x)

Bellovary, J. M., Hayoune, S., Chafra, K., et al. 2021, MNRAS, 505, 5129, doi: [10.1093/mnras/stab1665](https://doi.org/10.1093/mnras/stab1665)

Bennett, J. S., Sijacki, D., Costa, T., Laporte, N., & Witten, C. 2024, MNRAS, 527, 1033, doi: [10.1093/mnras/stad3179](https://doi.org/10.1093/mnras/stad3179)

Bhowmick, A. K., Blecha, L., Torrey, P., et al. 2022a, MNRAS, 510, 177, doi: [10.1093/mnras/stab3439](https://doi.org/10.1093/mnras/stab3439)

—. 2024a, MNRAS, 529, 3768, doi: [10.1093/mnras/stae780](https://doi.org/10.1093/mnras/stae780)

—. 2021, MNRAS, 507, 2012, doi: [10.1093/mnras/stab2204](https://doi.org/10.1093/mnras/stab2204)

Bhowmick, A. K., Blecha, L., Ni, Y., et al. 2022b, MNRAS, 516, 138, doi: [10.1093/mnras/stac2238](https://doi.org/10.1093/mnras/stac2238)

Bhowmick, A. K., Blecha, L., Torrey, P., et al. 2024b, MNRAS, 531, 4311, doi: [10.1093/mnras/stae1386](https://doi.org/10.1093/mnras/stae1386)

—. 2024c, MNRAS, 533, 1907, doi: [10.1093/mnras/stae1819](https://doi.org/10.1093/mnras/stae1819)

—. 2025a, MNRAS, 538, 518, doi: [10.1093/mnras/staf269](https://doi.org/10.1093/mnras/staf269)

Bhowmick, A. K., Blecha, L., Kelley, L. Z., et al. 2025b, arXiv e-prints, arXiv:2506.09184, <https://arxiv.org/abs/2506.09184>

Bird, S., Ni, Y., Tiziana Di M., et al. 2022, Monthly Notices of the Royal Astronomical Society, 512, 3703, doi: [10.1093/mnras/stac597](https://doi.org/10.1093/mnras/stac597)

Bogdán, Á., Goulding, A. D., Natarajan, P., et al. 2024, Nature Astronomy, 8, 126, doi: [10.1038/s41550-023-02111-9](https://doi.org/10.1038/s41550-023-02111-9)

Borodina, O., Ni, Y., Bennett, J. S., et al. 2025, ApJ, 981, 149, doi: [10.3847/1538-4357/adb016](https://doi.org/10.3847/1538-4357/adb016)

Bromm, V., & Loeb, A. 2003, ApJ, 596, 34, doi: [10.1086/377529](https://doi.org/10.1086/377529)

Byrne, L., Faucher-Giguère, C.-A., Stern, J., et al. 2023, MNRAS, 520, 722, doi: [10.1093/mnras/stad171](https://doi.org/10.1093/mnras/stad171)

Chabrier, G. 2003, PASP, 115, 763, doi: [10.1086/376392](https://doi.org/10.1086/376392)

Chen, N., Ni, Y., Tremmel, M., et al. 2022, MNRAS, 510, 531, doi: [10.1093/mnras/stab3411](https://doi.org/10.1093/mnras/stab3411)

Cho, H., Prather, B. S., Narayan, R., et al. 2023, ApJL, 959, L22, doi: [10.3847/2041-8213/ad1048](https://doi.org/10.3847/2041-8213/ad1048)

Cho, H., Prather, B. S., Su, K.-Y., Narayan, R., & Natarajan, P. 2024, ApJ, 977, 200, doi: [10.3847/1538-4357/ad9561](https://doi.org/10.3847/1538-4357/ad9561)

Costa, T., Sijacki, D., Trenti, M., & Haehnelt, M. G. 2014, MNRAS, 439, 2146, doi: [10.1093/mnras/stu101](https://doi.org/10.1093/mnras/stu101)

Damiano, A., Valentini, M., Borgani, S., et al. 2024, A&A, 692, A81, doi: [10.1051/0004-6361/202450021](https://doi.org/10.1051/0004-6361/202450021)

Das, A., Schleicher, D. R. G., Basu, S., & Boekholt, T. C. N. 2021a, MNRAS, doi: [10.1093/mnras/stab1428](https://doi.org/10.1093/mnras/stab1428)

Das, A., Schleicher, D. R. G., Leigh, N. W. C., & Boekholt, T. C. N. 2021b, MNRAS, 503, 1051, doi: [10.1093/mnras/stab402](https://doi.org/10.1093/mnras/stab402)

Davies, M. B., Miller, M. C., & Bellovary, J. M. 2011, ApJL, 740, L42, doi: [10.1088/2041-8205/740/2/L42](https://doi.org/10.1088/2041-8205/740/2/L42)

Dayal, P. 2024, A&A, 690, A182, doi: [10.1051/0004-6361/202451481](https://doi.org/10.1051/0004-6361/202451481)

Dekel, A., Stone, N. C., Chowdhury, D. D., et al. 2025, A&A, 695, A97, doi: [10.1051/0004-6361/202452393](https://doi.org/10.1051/0004-6361/202452393)

Di Matteo, T., Colberg, J., Springel, V., Hernquist, L., & Sijacki, D. 2008, The Astrophysical Journal, 676, 33, doi: [10.1086/524921](https://doi.org/10.1086/524921)

Dijkstra, M., Ferrara, A., & Mesinger, A. 2014, MNRAS, 442, 2036, doi: [10.1093/mnras/stu1007](https://doi.org/10.1093/mnras/stu1007)

Ding, X., Onoue, M., Silverman, J. D., et al. 2025, arXiv e-prints, arXiv:2505.03876, doi: [10.48550/arXiv.2505.03876](https://doi.org/10.48550/arXiv.2505.03876)

Dong-Páez, C. A., Volonteri, M., Dubois, Y., Beckmann, R. S., & Trebitsch, M. 2024, arXiv e-prints, arXiv:2412.02374, doi: [10.48550/arXiv.2412.02374](https://doi.org/10.48550/arXiv.2412.02374)

Durodola, E., Pacucci, F., & Hickox, R. C. 2024, arXiv e-prints, arXiv:2406.10329, doi: [10.48550/arXiv.2406.10329](https://doi.org/10.48550/arXiv.2406.10329)

Eilers, A.-C., Mackenzie, R., Pizzati, E., et al. 2024, ApJ, 974, 275, doi: [10.3847/1538-4357/ad778b](https://doi.org/10.3847/1538-4357/ad778b)

Fan, X., Narayanan, V. K., Lupton, R. H., et al. 2001, AJ, 122, 2833, doi: [10.1086/324111](https://doi.org/10.1086/324111)

Feng, Y., Di-Matteo, T., Croft, R. A., et al. 2016, MNRAS, 455, 2778, doi: [10.1093/mnras/stv2484](https://doi.org/10.1093/mnras/stv2484)

Finkelstein, S. L., Bagley, M. B., Ferguson, H. C., et al. 2023, ApJL, 946, L13, doi: [10.3847/2041-8213/acade4](https://doi.org/10.3847/2041-8213/acade4)

Fischer, M. S., & Sagunski, L. 2024, A&A, 690, A299, doi: [10.1051/0004-6361/202451304](https://doi.org/10.1051/0004-6361/202451304)

Fryer, C. L., Woosley, S. E., & Heger, A. 2001, ApJ, 550, 372, doi: [10.1086/319719](https://doi.org/10.1086/319719)

Genina, A., Springel, V., & Rantala, A. 2024, MNRAS, 534, 957, doi: [10.1093/mnras/stae2144](https://doi.org/10.1093/mnras/stae2144)

Goulding, A. D., Greene, J. E., Setton, D. J., et al. 2023, ApJL, 955, L24, doi: [10.3847/2041-8213/acf7c5](https://doi.org/10.3847/2041-8213/acf7c5)

Greene, J. E., Labbe, I., Goulding, A. D., et al. 2023, arXiv e-prints, arXiv:2309.05714, doi: [10.48550/arXiv.2309.05714](https://doi.org/10.48550/arXiv.2309.05714)

—. 2024, ApJ, 964, 39, doi: [10.3847/1538-4357/ad1e5f](https://doi.org/10.3847/1538-4357/ad1e5f)

Guo, M., Stone, J. M., Quataert, E., & Kim, C.-G. 2024, ApJ, 973, 141, doi: [10.3847/1538-4357/ad5fe7](https://doi.org/10.3847/1538-4357/ad5fe7)

Habouzit, M., Volonteri, M., & Dubois, Y. 2017, MNRAS, 468, 3935, doi: [10.1093/mnras/stx666](https://doi.org/10.1093/mnras/stx666)

Habouzit, M., Volonteri, M., Latif, M., Dubois, Y., & Peirani, S. 2016, MNRAS, 463, 529, doi: [10.1093/mnras/stw1924](https://doi.org/10.1093/mnras/stw1924)

Harikane, Y., Zhang, Y., Nakajima, K., et al. 2023, ApJ, 959, 39, doi: [10.3847/1538-4357/ad029e](https://doi.org/10.3847/1538-4357/ad029e)

Henden, N. A., Puchwein, E., Shen, S., & Sijacki, D. 2018, MNRAS, 479, 5385, doi: [10.1093/mnras/sty1780](https://doi.org/10.1093/mnras/sty1780)

Hoffman, Y., & Ribak, E. 1991, ApJL, 380, L5, doi: [10.1086/186160](https://doi.org/10.1086/186160)

Huang, K.-W., Ni, Y., Feng, Y., & Di Matteo, T. 2020, MNRAS, 496, 1, doi: [10.1093/mnras/staa1515](https://doi.org/10.1093/mnras/staa1515)

Jeon, J., Liu, B., Taylor, A. J., et al. 2025, ApJ, 988, 110, doi: [10.3847/1538-4357/ade2e1](https://doi.org/10.3847/1538-4357/ade2e1)

Jiang, L., McGreer, I. D., Fan, X., et al. 2016, ApJ, 833, 222, doi: [10.3847/1538-4357/833/2/222](https://doi.org/10.3847/1538-4357/833/2/222)

Jiang, Y.-F., Stone, J. M., & Davis, S. W. 2019, ApJ, 880, 67, doi: [10.3847/1538-4357/ab29ff](https://doi.org/10.3847/1538-4357/ab29ff)

Juodžbalis, I., Maiolino, R., Baker, W. M., et al. 2025, arXiv e-prints, arXiv:2504.03551, doi: [10.48550/arXiv.2504.03551](https://doi.org/10.48550/arXiv.2504.03551)

Kannan, R., Garaldi, E., Smith, A., et al. 2022, MNRAS, 511, 4005, doi: [10.1093/mnras/stab3710](https://doi.org/10.1093/mnras/stab3710)

Kannan, R., Springel, V., Hernquist, L., et al. 2023, MNRAS, 524, 2594, doi: [10.1093/mnras/stac3743](https://doi.org/10.1093/mnras/stac3743)

Katz, N., Weinberg, D. H., & Hernquist, L. 1996, ApJS, 105, 19, doi: [10.1086/192305](https://doi.org/10.1086/192305)

Kelley, L. Z., Blecha, L., & Hernquist, L. 2017, MNRAS, 464, 3131, doi: [10.1093/mnras/stw2452](https://doi.org/10.1093/mnras/stw2452)

Khanda, N., Di Matteo, T., Croft, R., et al. 2015, MNRAS, 450, 1349, doi: [10.1093/mnras/stv627](https://doi.org/10.1093/mnras/stv627)

Kocevski, D. D., Onoue, M., Inayoshi, K., et al. 2023, ApJL, 954, L4, doi: [10.3847/2041-8213/ace5a0](https://doi.org/10.3847/2041-8213/ace5a0)

Kocevski, D. D., Finkelstein, S. L., Barro, G., et al. 2024, arXiv e-prints, arXiv:2404.03576, doi: [10.48550/arXiv.2404.03576](https://doi.org/10.48550/arXiv.2404.03576)

Kokorev, V., Fujimoto, S., Labbe, I., et al. 2023, ApJL, 957, L7, doi: [10.3847/2041-8213/ad037a](https://doi.org/10.3847/2041-8213/ad037a)

Kokorev, V., Caputi, K. I., Greene, J. E., et al. 2024, ApJ, 968, 38, doi: [10.3847/1538-4357/ad4265](https://doi.org/10.3847/1538-4357/ad4265)

Kovács, O. E., Bogdán, Á., Natarajan, P., et al. 2024, ApJL, 965, L21, doi: [10.3847/2041-8213/ad391f](https://doi.org/10.3847/2041-8213/ad391f)

Kroupa, P., Subr, L., Jerabkova, T., & Wang, L. 2020, MNRAS, 498, 5652, doi: [10.1093/mnras/staa2276](https://doi.org/10.1093/mnras/staa2276)

Larson, R. L., Finkelstein, S. L., Kocevski, D. D., et al. 2023, ApJL, 953, L29, doi: [10.3847/2041-8213/ace619](https://doi.org/10.3847/2041-8213/ace619)

Latif, M. A., Schleicher, D. R. G., & Hartwig, T. 2016, MNRAS, 458, 233, doi: [10.1093/mnras/stw297](https://doi.org/10.1093/mnras/stw297)

Latif, M. A., Schleicher, D. R. G., & Khochfar, S. 2023, ApJ, 945, 137, doi: [10.3847/1538-4357/acbcc2](https://doi.org/10.3847/1538-4357/acbcc2)

Li, K., Volonteri, M., Dubois, Y., Beckmann, R., & Trebitsch, M. 2024, arXiv e-prints, arXiv:2410.07856, doi: [10.48550/arXiv.2410.07856](https://doi.org/10.48550/arXiv.2410.07856)

Luo, Y., Ardaneh, K., Shlosman, I., et al. 2018, MNRAS, 476, 3523, doi: [10.1093/mnras/sty362](https://doi.org/10.1093/mnras/sty362)

Luo, Y., Shlosman, I., Nagamine, K., & Fang, T. 2020, MNRAS, 492, 4917, doi: [10.1093/mnras/staa153](https://doi.org/10.1093/mnras/staa153)

Lupi, A. 2024, in EAS2024, European Astronomical Society Annual Meeting, 724

Lupi, A., Colpi, M., Devecchi, B., Galanti, G., & Volonteri, M. 2014, MNRAS, 442, 3616, doi: [10.1093/mnras/stu1120](https://doi.org/10.1093/mnras/stu1120)

Ma, L., Hopkins, P. F., Kelley, L. Z., & Faucher-Giguère, C.-A. 2023, MNRAS, 519, 5543, doi: [10.1093/mnras/stad036](https://doi.org/10.1093/mnras/stad036)

Madau, P., & Rees, M. J. 2001, ApJL, 551, L27, doi: [10.1086/319848](https://doi.org/10.1086/319848)

Maiolino, R., Scholtz, J., Curtis-Lake, E., et al. 2023, arXiv e-prints, arXiv:2308.01230, doi: [10.48550/arXiv.2308.01230](https://doi.org/10.48550/arXiv.2308.01230)

Maiolino, R., Scholtz, J., Witstok, J., et al. 2024, Nature, 627, 59, doi: [10.1038/s41586-024-07052-5](https://doi.org/10.1038/s41586-024-07052-5)

Massonneau, W., Volonteri, M., Dubois, Y., & Beckmann, R. S. 2023, A&A, 670, A180, doi: [10.1051/0004-6361/202243170](https://doi.org/10.1051/0004-6361/202243170)

Matsuoka, Y., Iwasawa, K., Onoue, M., et al. 2018, ApJS, 237, 5, doi: [10.3847/1538-4365/aac724](https://doi.org/10.3847/1538-4365/aac724)

Matsuoka, Y., Onoue, M., Kashikawa, N., et al. 2019, ApJL, 872, L2, doi: [10.3847/2041-8213/ab0216](https://doi.org/10.3847/2041-8213/ab0216)

Mayer, L., Capelo, P. R., Zwick, L., & Di Matteo, T. 2024, ApJ, 961, 76, doi: [10.3847/1538-4357/ad11cf](https://doi.org/10.3847/1538-4357/ad11cf)

Mehta, D., Regan, J. A., & Prole, L. 2024, The Open Journal of Astrophysics, 7, 107, doi: [10.33232/001c.126629](https://doi.org/10.33232/001c.126629)

Merritt, D. 2013, Classical and Quantum Gravity, 30, 244005, doi: [10.1088/0264-9381/30/24/244005](https://doi.org/10.1088/0264-9381/30/24/244005)

Mortlock, D. J., Warren, S. J., Venemans, B. P., et al. 2011, Nature, 474, 616, doi: [10.1038/nature10159](https://doi.org/10.1038/nature10159)

Mukherjee, D., Zhou, Y., Chen, N., Di Carlo, U. N., & Di Matteo, T. 2024, arXiv e-prints, arXiv:2409.19095, doi: [10.48550/arXiv.2409.19095](https://doi.org/10.48550/arXiv.2409.19095)

Mushotzky, R. F., Aird, J., Barger, A. J., et al. 2019, The Advanced X-ray Imaging Satellite. <https://arxiv.org/abs/1903.04083>

Naidu, R. P., Matthee, J., Katz, H., et al. 2025, arXiv e-prints, arXiv:2503.16596, doi: [10.48550/arXiv.2503.16596](https://doi.org/10.48550/arXiv.2503.16596)

Narayanan, D., Lower, S., Torrey, P., et al. 2024, ApJ, 961, 73, doi: [10.3847/1538-4357/ad0966](https://doi.org/10.3847/1538-4357/ad0966)

Natarajan, P. 2011, Bulletin of the Astronomical Society of India, 39, 145, doi: [10.48550/arXiv.1104.4797](https://doi.org/10.48550/arXiv.1104.4797)

—. 2021, MNRAS, 501, 1413, doi: [10.1093/mnras/staa3724](https://doi.org/10.1093/mnras/staa3724)

Natarajan, P., Pacucci, F., Ferrara, A., et al. 2017, ApJ, 838, 117, doi: [10.3847/1538-4357/aa6330](https://doi.org/10.3847/1538-4357/aa6330)

Natarajan, P., Pacucci, F., Ricarte, A., et al. 2024, ApJL, 960, L1, doi: [10.3847/2041-8213/ad0e76](https://doi.org/10.3847/2041-8213/ad0e76)

Nelson, D., Springel, V., Pillepich, A., et al. 2019, Computational Astrophysics and Cosmology, 6, 2, doi: [10.1186/s40668-019-0028-x](https://doi.org/10.1186/s40668-019-0028-x)

Ni, Y., Chen, N., Zhou, Y., et al. 2024, The Astrid Simulation: Evolution of black holes and galaxies to  $z=0.5$  and different evolution pathways for galaxy quenching. <https://arxiv.org/abs/2409.10666>

Ni, Y., Di Matteo, T., & Feng, Y. 2022, MNRAS, 509, 3043, doi: [10.1093/mnras/stab3162](https://doi.org/10.1093/mnras/stab3162)

Ni, Y., Tiziana Di M., Bird, S., et al. 2022, Monthly Notices of the Royal Astronomical Society, 513, 670, doi: [10.1093/mnras/stac1329](https://doi.org/10.1093/mnras/stac1329)

O'Brennan, H., Regan, J. A., Brennan, J., et al. 2025, arXiv e-prints, arXiv:2502.00574, doi: [10.48550/arXiv.2502.00574](https://doi.org/10.48550/arXiv.2502.00574)

Onoue, M., Inayoshi, K., Ding, X., et al. 2023, ApJL, 942, L17, doi: [10.3847/2041-8213/aca9d3](https://doi.org/10.3847/2041-8213/aca9d3)

Onoue, M., Ding, X., Silverman, J. D., et al. 2024, arXiv e-prints, arXiv:2409.07113, doi: [10.48550/arXiv.2409.07113](https://doi.org/10.48550/arXiv.2409.07113)

Pakmor, R., Bauer, A., & Springel, V. 2011, MNRAS, 418, 1392, doi: [10.1111/j.1365-2966.2011.19591.x](https://doi.org/10.1111/j.1365-2966.2011.19591.x)

Pakmor, R., Pfrommer, C., Simpson, C. M., Kannan, R., & Springel, V. 2016, MNRAS, 462, 2603, doi: [10.1093/mnras/stw1761](https://doi.org/10.1093/mnras/stw1761)

Pakmor, R., Springel, V., Coles, J. P., et al. 2023, MNRAS, 524, 2539, doi: [10.1093/mnras/stac3620](https://doi.org/10.1093/mnras/stac3620)

Partmann, C., Naab, T., Lahén, N., et al. 2025, MNRAS, 537, 956, doi: [10.1093/mnras/staf002](https://doi.org/10.1093/mnras/staf002)

Petersson, J., Hirschmann, M., Tress, R. G., et al. 2025, arXiv e-prints, arXiv:2504.08035, doi: [10.48550/arXiv.2504.08035](https://doi.org/10.48550/arXiv.2504.08035)

Pfister, H., Volonteri, M., Dubois, Y., Dotti, M., & Colpi, M. 2019, MNRAS, 486, 101, doi: [10.1093/mnras/stz822](https://doi.org/10.1093/mnras/stz822)

Pillepich, A., Springel, V., Nelson, D., et al. 2018a, MNRAS, 473, 4077, doi: [10.1093/mnras/stx2656](https://doi.org/10.1093/mnras/stx2656)

Pillepich, A., Nelson, D., Hernquist, L., et al. 2018b, MNRAS, 475, 648, doi: [10.1093/mnras/stx3112](https://doi.org/10.1093/mnras/stx3112)

Planck Collaboration, Ade, P. A. R., Aghanim, N., et al. 2016, A&A, 594, A13, doi: [10.1051/0004-6361/201525830](https://doi.org/10.1051/0004-6361/201525830)

Prole, L. R., Regan, J. A., Whalen, D. J., Glover, S. C. O., & Klessen, R. S. 2024, A&A, 692, A213, doi: [10.1051/0004-6361/202452486](https://doi.org/10.1051/0004-6361/202452486)

Ramos Padilla, A. F., Ashby, M. L. N., Smith, H. A., et al. 2020, MNRAS, 499, 4325, doi: [10.1093/mnras/staa2813](https://doi.org/10.1093/mnras/staa2813)

Reed, S. L., McMahon, R. G., Martini, P., et al. 2017, MNRAS, 468, 4702, doi: [10.1093/mnras/stx728](https://doi.org/10.1093/mnras/stx728)

Regan, J. A., Johansson, P. H., & Wise, J. H. 2014, ApJ, 795, 137, doi: [10.1088/0004-637X/795/2/137](https://doi.org/10.1088/0004-637X/795/2/137)

Regan, J. A., Wise, J. H., O’Shea, B. W., & Norman, M. L. 2020a, MNRAS, 492, 3021, doi: [10.1093/mnras/staa035](https://doi.org/10.1093/mnras/staa035)

Regan, J. A., Wise, J. H., Woods, T. E., et al. 2020b, The Open Journal of Astrophysics, 3, 15, doi: [10.21105/astro.2008.08090](https://doi.org/10.21105/astro.2008.08090)

Rusakov, V., Watson, D., Nikopoulos, G. P., et al. 2025, arXiv e-prints, arXiv:2503.16595, doi: [10.48550/arXiv.2503.16595](https://doi.org/10.48550/arXiv.2503.16595)

Sassano, F., Schneider, R., Valiante, R., et al. 2021, MNRAS, 506, 613, doi: [10.1093/mnras/stab1737](https://doi.org/10.1093/mnras/stab1737)

Satheesh, P., Blecha, L., & Kelley, L. Z. 2025, arXiv e-prints, arXiv:2506.04369, doi: [10.48550/arXiv.2506.04369](https://doi.org/10.48550/arXiv.2506.04369)

Sayeb, M., Blecha, L., Kelley, L. Z., et al. 2021, MNRAS, 501, 2531, doi: [10.1093/mnras/staa3826](https://doi.org/10.1093/mnras/staa3826)

Schneider, R., Valiante, R., Trinca, A., et al. 2023, MNRAS, 526, 3250, doi: [10.1093/mnras/stad2503](https://doi.org/10.1093/mnras/stad2503)

Scoggins, M. T., & Haiman, Z. 2024, MNRAS, 531, 4584, doi: [10.1093/mnras/stae1449](https://doi.org/10.1093/mnras/stae1449)

Scoggins, M. T., Haiman, Z., & Wise, J. H. 2023, MNRAS, 519, 2155, doi: [10.1093/mnras/stac3715](https://doi.org/10.1093/mnras/stac3715)

Shang, C., Bryan, G. L., & Haiman, Z. 2010, MNRAS, 402, 1249, doi: [10.1111/j.1365-2966.2009.15960.x](https://doi.org/10.1111/j.1365-2966.2009.15960.x)

Shen, X., Hopkins, P. F., Faucher-Giguère, C.-A., et al. 2020, MNRAS, 495, 3252, doi: [10.1093/mnras/staa1381](https://doi.org/10.1093/mnras/staa1381)

Sijacki, D., Springel, V., & Haehnelt, M. G. 2009, MNRAS, 400, 100, doi: [10.1111/j.1365-2966.2009.15452.x](https://doi.org/10.1111/j.1365-2966.2009.15452.x)

Sivasankaran, A., Blecha, L., Torrey, P., et al. 2025, MNRAS, 537, 817, doi: [10.1093/mnras/staf062](https://doi.org/10.1093/mnras/staf062)

Siwek, M., Kelley, L. Z., & Hernquist, L. 2024, MNRAS, 534, 2609, doi: [10.1093/mnras/stae2251](https://doi.org/10.1093/mnras/stae2251)

Siwek, M., Weinberger, R., & Hernquist, L. 2023, MNRAS, 522, 2707, doi: [10.1093/mnras/stad1131](https://doi.org/10.1093/mnras/stad1131)

Sądowski, A., & Narayan, R. 2016, MNRAS, 456, 3929, doi: [10.1093/mnras/stv2941](https://doi.org/10.1093/mnras/stv2941)

Smith, B., Sigurdsson, S., & Abel, T. 2008, MNRAS, 385, 1443, doi: [10.1111/j.1365-2966.2008.12922.x](https://doi.org/10.1111/j.1365-2966.2008.12922.x)

Smith, B. D., Regan, J. A., Downes, T. P., et al. 2018, MNRAS, 480, 3762, doi: [10.1093/mnras/sty2103](https://doi.org/10.1093/mnras/sty2103)

Springel, V. 2010, MNRAS, 401, 791, doi: [10.1111/j.1365-2966.2009.15715.x](https://doi.org/10.1111/j.1365-2966.2009.15715.x)

Springel, V., & Hernquist, L. 2003, MNRAS, 339, 289, doi: [10.1046/j.1365-8711.2003.06206.x](https://doi.org/10.1046/j.1365-8711.2003.06206.x)

Su, K.-Y., Natarajan, P., Cho, H., et al. 2025, ApJL, 981, L33, doi: [10.3847/2041-8213/adb7dd](https://doi.org/10.3847/2041-8213/adb7dd)

Sugimura, K., Omukai, K., & Inoue, A. K. 2014, MNRAS, 445, 544, doi: [10.1093/mnras/stu1778](https://doi.org/10.1093/mnras/stu1778)

Taylor, A. J., Kokorev, V., Kocevski, D. D., et al. 2025, ApJL, 989, L7, doi: [10.3847/2041-8213/ade789](https://doi.org/10.3847/2041-8213/ade789)

Torrey, P., Vogelsberger, M., Genel, S., et al. 2014, MNRAS, 438, 1985, doi: [10.1093/mnras/stt2295](https://doi.org/10.1093/mnras/stt2295)

Trakhtenbrot, B., Volonteri, M., & Natarajan, P. 2017, ApJL, 836, L1, doi: [10.3847/2041-8213/836/1/L1](https://doi.org/10.3847/2041-8213/836/1/L1)

Tremmel, M., Governato, F., Volonteri, M., & Quinn, T. R. 2015, MNRAS, 451, 1868, doi: [10.1093/mnras/stv1060](https://doi.org/10.1093/mnras/stv1060)

Tremmel, M., Karcher, M., Governato, F., et al. 2017, MNRAS, 470, 1121, doi: [10.1093/mnras/stx1160](https://doi.org/10.1093/mnras/stx1160)

Trinca, A., Schneider, R., Valiante, R., et al. 2022, MNRAS, 511, 616, doi: [10.1093/mnras/stac062](https://doi.org/10.1093/mnras/stac062)

Trinca, A., Valiante, R., Schneider, R., et al. 2024, arXiv e-prints, arXiv:2412.14248, doi: [10.48550/arXiv.2412.14248](https://doi.org/10.48550/arXiv.2412.14248)

Valiante, R., Schneider, R., Volonteri, M., & Omukai, K. 2016, MNRAS, 457, 3356, doi: [10.1093/mnras/stw225](https://doi.org/10.1093/mnras/stw225)

van de Weygaert, R., & Bertschinger, E. 1996, MNRAS, 281, 84, doi: [10.1093/mnras/281.1.84](https://doi.org/10.1093/mnras/281.1.84)

Venemans, B. P., Verdoes Kleijn, G. A., Mwebaze, J., et al. 2015, MNRAS, 453, 2259, doi: [10.1093/mnras/stv1774](https://doi.org/10.1093/mnras/stv1774)

Visbal, E., & Haiman, Z. 2018, ApJL, 865, L9, doi: [10.3847/2041-8213/aadf3a](https://doi.org/10.3847/2041-8213/aadf3a)

Vogelsberger, M., Genel, S., Sijacki, D., et al. 2013, MNRAS, 436, 3031, doi: [10.1093/mnras/stt1789](https://doi.org/10.1093/mnras/stt1789)

Vogelsberger, M., Genel, S., Springel, V., et al. 2014a, MNRAS, 444, 1518, doi: [10.1093/mnras/stu1536](https://doi.org/10.1093/mnras/stu1536)

—. 2014b, Nature, 509, 177, doi: [10.1038/nature13316](https://doi.org/10.1038/nature13316)

Vogelsberger, M., Nelson, D., Pillepich, A., et al. 2020, MNRAS, 492, 5167, doi: [10.1093/mnras/staa137](https://doi.org/10.1093/mnras/staa137)

Volonteri, M., Silk, J., & Dubus, G. 2015, ApJ, 804, 148, doi: [10.1088/0004-637X/804/2/148](https://doi.org/10.1088/0004-637X/804/2/148)

Wang, F., Yang, J., Fan, X., et al. 2018, ApJL, 869, L9, doi: [10.3847/2041-8213/aafl02](https://doi.org/10.3847/2041-8213/aafl02)

—. 2021, ApJL, 907, L1, doi: [10.3847/2041-8213/abd8c6](https://doi.org/10.3847/2041-8213/abd8c6)

Ward, S. R., Costa, T., Harrison, C. M., & Mainieri, V. 2024, MNRAS, 533, 1733, doi: [10.1093/mnras/stae1816](https://doi.org/10.1093/mnras/stae1816)

Weinberger, R., Bhowmick, A., Blecha, L., et al. 2025, arXiv e-prints, arXiv:2502.13241, doi: [10.48550/arXiv.2502.13241](https://doi.org/10.48550/arXiv.2502.13241)

Weinberger, R., Springel, V., & Pakmor, R. 2020, ApJS, 248, 32, doi: [10.3847/1538-4365/ab908c](https://doi.org/10.3847/1538-4365/ab908c)

Weinberger, R., Springel, V., Hernquist, L., et al. 2017, MNRAS, 465, 3291, doi: [10.1093/mnras/stw2944](https://doi.org/10.1093/mnras/stw2944)

Wiersma, R. P. C., Schaye, J., & Smith, B. D. 2009, MNRAS, 393, 99, doi: [10.1111/j.1365-2966.2008.14191.x](https://doi.org/10.1111/j.1365-2966.2008.14191.x)

Willott, C. J., Delorme, P., Reylé, C., et al. 2010, AJ, 139, 906, doi: [10.1088/0004-6256/139/3/906](https://doi.org/10.1088/0004-6256/139/3/906)

Wise, J. H., Regan, J. A., O’Shea, B. W., et al. 2019, Nature, 566, 85, doi: [10.1038/s41586-019-0873-4](https://doi.org/10.1038/s41586-019-0873-4)

Xu, H., Wise, J. H., & Norman, M. L. 2013, *ApJ*, 773, 83,  
doi: [10.1088/0004-637X/773/2/83](https://doi.org/10.1088/0004-637X/773/2/83)

Yang, J., Wang, F., Fan, X., et al. 2019, *AJ*, 157, 236,  
doi: [10.3847/1538-3881/ab1be1](https://doi.org/10.3847/1538-3881/ab1be1)

Yu, Q., & Tremaine, S. 2002, *MNRAS*, 335, 965,  
doi: [10.1046/j.1365-8711.2002.05532.x](https://doi.org/10.1046/j.1365-8711.2002.05532.x)

Zhu, Q., Li, Y., Li, Y., et al. 2022, *MNRAS*, 514, 5583,  
doi: [10.1093/mnras/stac1556](https://doi.org/10.1093/mnras/stac1556)